Ab Initio Study of the Electronic Structure of Co adatom on Cu(111) Surface

by

Arefa Hossain

B.Sc., The University of Dhaka, 2001

A THESIS SUBMITTED IN PARTIAL FULFILMENT OF
THE REQUIREMENTS FOR THE DEGREE OF

MASTER OF SCIENCE

in

The Faculty of Graduate Studies

(Physics)

THE UNIVERSITY OF BRITISH COLUMBIA

October 17, 2005

Abstract

We present the *ab initio* Density Functional study of the electronic structure of Co adatoms on Cu(111) surface. A number of Scanning Tunneling Spectroscopy (STS) experiments performed on the systems which contain magnetic adatoms on the noble metal surfaces (e.g., Co, Ce on Cu, Ag, Au (111) planes) [1, 6, 7] report the observation of intriguing resonances at the Fermi energy. However, the interpretation of these experiments in terms of the Kondo physics is not totally conclusive and gave rise to many questions that are still to be answered. The first step towards understanding the meaning of these experiments is to understand the electronic structure of such systems. The so called supercell approximation is used to simulate a Cu slab consisting of Cu(111) planes. The electronic properties of Co adatom on Cu(111) surface is studied in a symmetric 2×2 supercell in the xy directions with fifteen Cu(111) and two Co planes in the z direction. It is observed that Co is in the d^8 high spin state with the magnetic moment of 1.7 μ_B per Co atom. The width of Co d DOS is a result of the coupling with the Cu sp surface and bulk states. At least the first three Cu layers of the bulk Cu slab have significant influence on the electronic properties of Co.

Contents

List of Figures

Acknowledgements

Chapter 1

Introduction

Crystal surfaces are very special because they break the translational symmetry and thereby introduce different potentials at the crystal boundary as compared to the bulk. This changes the electronic structure near the surface, leading to new, potentially interesting material properties. The special surface environment of a metallic crystal can be pushed to a more exotic limit by introducing magnetic impurities on them. Interaction of the quasi two-dimensional electron gas at the surface with the net spin of the magnetic impurity can bring the system into novel ground states that are currently a topic of intense research, both theoretical and experimental.

Apart from their fundamental scientific importance, these systems are also of great technological importance. The miniaturization and increase in speed of electronic devices is fast approaching the limit where quantum effects interfere with the normal operation of the device. At this limit the future of the electronic industry is in great need of exploiting the fundamental interactions that govern the behavior of electrons in the solid.

A recent series of scanning tunneling spectroscopy experiments with clever manipulations of magnetic atoms on various metal surfaces [1, 6, 7, 8] has produced some very intriguing results. Among these experiments, most notable is the 'quantum mirage' experiment [1] where Manoharan *et al* studied an elliptical quantum confinement or corral built with magnetic atoms (Co) placed on a Cu(111) surface. The issues addressed by the experiments are directly related to the general nature of electron correlations between the conduction electrons of a metal and their interactions with surface impurities. Therefore, it is important, for both fundamental science and technologies, to carefully examine the results and the current interpretations of these experiments. In reality the results of the experiments which we shall discuss at length in the later part of the chapter, generated more questions than they answered. This motivated us to look at the electronic structure of Co impurities deposited on Cu(111) surfaces starting from a very detailed study of the electronic structure of pure Cu(111) plane.

Chapter 1 of the thesis starts with a very general introduction to the nature of the interactions of conduction electrons with the localized impurity states and Kondo physics. This is followed by a discussion of how to interpret STM spectra, in particular, the relation between dI/dV spectra and densities of states of the system. This discussion helps us to understand the justification behind the earlier STM observation of the Kondo resonance. After setting up the ground work we discuss the very

important STM experiments done by Manoharan *et al* [1] and some problems with the current interpretation of the experimental results.

1.1 The Anderson impurity model and the Kondo effect

The simplest model of a local magnetic moment associated with a spin $S = 1/2$ impurity in a metallic host is known as the Anderson impurity model [2]. The Anderson model starts with the Hamiltonian for the system of local magnetic moment in a metallic host:

$$H_{Anderson} = \sum_{\mathbf{k},\sigma} \epsilon_{\mathbf{k},\sigma} c_{\mathbf{k},\sigma}^\dagger c_{\mathbf{k},\sigma} + \sum_\sigma \epsilon_{d,\sigma} d_\sigma^\dagger d_\sigma + U d_{\sigma\uparrow}^\dagger d_{\sigma\uparrow} d_{\sigma\downarrow}^\dagger d_{\sigma\downarrow}$$
$$+ \sum_{\mathbf{k},\sigma} (V_{\mathbf{k}d,\sigma} c_{\mathbf{k},\sigma}^\dagger d_\sigma + h.c.) \tag{1.1}$$

where the first term represents the energy of the noninteracting electrons of the Fermi sea, the second term represents the energy of an electron in the localized d or f level, the third term represents an on-site repulsion if two electrons try to occupy the localized level and the last term represents coupling between the d-level and the conduction electrons. Also $c_{\mathbf{k},\sigma}^\dagger (c_{\mathbf{k},\sigma})$ is the creation(annihilation) operator of an electron in the Fermi sea with wave vector k and spin σ and $d_\sigma^\dagger (d_\sigma)$ is the creation(annihilation) operator of an electron in the localized d or f level with spin σ. U is the energy required for adding a second electron of opposite spin to the impurity level and $V_{\mathbf{k}d,\sigma}$ is the $\mathbf{k}$ dependent hopping parameter for connecting the electrons of the fermi sea to the localized impurity level.

In the literature a single magnetic impurity in a nonmagnetic host is often referred to as a Kondo impurity. At sufficiently low temperature, the spin of the Kondo impurity interacts with the spin of the surrounding conduction electrons (causing spin-flip scattering) which results in a change of the temperature dependence of the resistivity notably a minimum in the resistivity at a characteristic temperature. This phenomenon is known as the Kondo effect. In other words, the Kondo effect is the many body response of the free electrons in the Fermi sea to the magnetic impurity.

From the Anderson Hamiltonian one finds out that even for a small value of $V_{\mathbf{k}d,\sigma}$ the singly and doubly occupied states of the local level broadens by an amount $\Gamma \approx 2\pi |V_{\mathbf{k}d,\sigma}|^2 \rho_0$ as given by Fermi's Golden rule where ρ_0 is the density of conduction electrons at the Fermi energy. In the regime $\epsilon_d < E_F$ and $\epsilon_d + U > E_F$, the ground state of the impurity is always singly occupied therefore one has a magnetic impurity here. This regime of magnetic impurity is of central interest for the Kondo

problem. Anderson showed that Eq. 1.1 will lead to local moment formation when $\Gamma \approx 2\pi |V_{kd,\sigma}|^2 \rho_0 \ll |\epsilon_d|, \epsilon_d + U$.

Using a canonical transformation in the local moment regime of the Anderson model, Schrieffer and Wolff [5] showed that the Anderson Hamiltonian (Eq. 1.1) can be transformed to the Kondo Hamiltonian with an energy-dependent exchange interaction $J_{kk'}$. The Kondo Hamiltonian describes the scattering of conduction electrons by a localized impurity spin in terms of the exchange interaction $J_{kk'}$ which is

$$H_{Kondo-exchange} = \sum_{\mathbf{k},\mathbf{k'}} J_{\mathbf{k},\mathbf{k'}}(\Psi_{\mathbf{k'}}^\dagger S \Psi_{\mathbf{k}}) \cdot (\Psi_d^\dagger S \Psi_d). \tag{1.2}$$

where field operators are $\Psi_{\mathbf{k}} = \begin{pmatrix} c_{\mathbf{k}\uparrow} \\ c_{\mathbf{k}\downarrow} \end{pmatrix}$, $\Psi_d = \begin{pmatrix} c_{d\uparrow} \\ c_{d\downarrow} \end{pmatrix}$ and $2S = \sigma$ are the Pauli matrices. The form of $J_{kk'}$ is also calculated by Schrieffer and Wolff [5]:

$$J_{\mathbf{k}\mathbf{k'}} = V_{kd}^* V_{k'd} \left\{ \frac{1}{\epsilon_k - \epsilon_d - U} + \frac{1}{\epsilon_{k'} - \epsilon_d - U} - \frac{1}{\epsilon_k - \epsilon_d} - \frac{1}{\epsilon_{k'} - \epsilon_d} \right\}. \tag{1.3}$$

At sufficiently low temperature (i.e., temperatures below a characteristic Kondo temperature T_K, defined below) the spin of the conduction electrons together with the local moment tend to form a many body spin singlet ground state that collectively screens the local spin of the Kondo impurity. In this situation, if the spin of the magnetic ion is 1/2, the Kondo effect completely screens the ion spin at sufficiently large distances. This spin compensation in the conduction electron gas is usually called the 'spin compensation cloud' or 'Kondo cloud'. This means that the spin-flip scattering is frozen-out and we can treat the scattering as purely potential scattering. The impurity density of states (i.e. the density of states of the atomic d or f levels that give rise to the magnetic moment) develops a narrow DOS peak near the Fermi energy and this is called the Abrikosov-Shul resonance or Kondo resonance [3, 4]. The impurity density of states of the Anderson model in the local-moment regime is shown in Fig. 9 of [9].

Now we should emphasize the following points which have central importance to our work:

1. In the Kondo model a characteristic temperature T_K, known as Kondo temperature, is given by

$$T_K \propto \exp(-\frac{1}{2J\rho_0}) \tag{1.4}$$

where $J(J > 0)$ is the antiferromagnetic coupling between the impurity spin and the spin of the host electrons that has been approximated as $\mathbf{k}$ independent. ρ_0 is the density of states at the Fermi level. We already mentioned that at $T \approx T_K$ a spin compensation cloud is built up around the magnetic impurity. By noticing that

only those electrons are strongly scattered by the impurity whose energy is not much further from the Fermi level than the characteristic Kondo energy $k_B T_K$, one can realize that the spatial extension of this compensation cloud may be characterized by the 'coherence length' of the Kondo problem:

$$\xi = \frac{v_F}{k_B T_K} \tag{1.5}$$

where v_F is the Fermi velocity and k_B is the Boltzmann constant. In the Kondo effect, the narrow resonance appearing in the scattering amplitude has the width $k_B T_K$. Since $k_B T_K$ can be small, the corresponding coherence length ξ_{kT_K} is rather large. We should note that because of the large spatial extend of the Kondo cloud of electrons the effective impurity has become very large. It is this extra scattering at low temperatures that causes the resistivity to increase with decreasing temperature below the Kondo temperature.

2. We have seen that, in case of Anderson Hamiltonian, even for a small value of $V_{\mathbf{k}d}$ the singly and doubly occupied states of the local level broadens by an amount $\Gamma \approx 2\pi |V_{\mathbf{k}d}|^2 \rho_0$.

The broadening of the localized states is originated from the one-electron scattering processes between the localized states and conduction electrons. This can be described by the localized state Green function $G_{d,\sigma}(\omega)$ renormalized by the Coulomb repulsion. Thus the scattering (non-spin-flip) amplitude of the conduction electrons with incoming and outgoing momenta $\mathbf{k}$ and $\mathbf{k}'$, respectively can be expressed as:

$$t_{\mathbf{k}\mathbf{k}',\sigma}(\omega) = V_{\mathbf{k}d} G_{d,\sigma}(\omega) V_{d\mathbf{k}'} \tag{1.6}$$

Taking the imaginary part of Eqn. 1.6 with $\mathbf{k} = \mathbf{k}'$ one can arrive at:

$$\mathrm{Im} t_{\mathbf{k}\mathbf{k},\sigma}(\omega) = \pi |V_{\mathbf{k}d}|^2 \rho_{d,\sigma}(\omega). \tag{1.7}$$

This equation plays a central role in our approach to the problem because according to the 'optical theorem' the total scattering cross section is proportional to the imaginary part of the forward scattering amplitude $t_{\mathbf{k}\mathbf{k},\sigma}(\omega)$, and therefore it is proportional to $\rho_{d,\sigma}(\omega)$. This connection is the reason for choosing to calculate the density of states of the localized states. We shall say more about this in Chapter 4.

1.2 Introduction to Scanning tunneling microscopy

Several STM experiments done on metal surfaces with embedded magnetic atoms have observed a sharp suppression in the differential conductance dI/dV when the STM tip is in the immediate vicinity of the magnetic impurity and the voltage is close

to zero [6, 7, 1, 13, 15]. This sharp suppression has been attributed as a manifestation of the Kondo resonance around the magnetic atom. To understand 'how' and 'what' is being observed by the dI/dV spectra one first needs to know about the tunneling mechanism in the STM measurements. The treatment presented here closely follows Fiete *et al* [9].

The basic tunneling geometry and energy diagram is shown in Fig. 1 of [15]. One can take the STM data in two different ways. One is called the 'constant current' method when the total current is kept constant by changing the height of the tip above the surface with the applied voltage. The data taken in this method is called the 'topographic image' of the sample that is being scanned. The other type of measurements are called 'constant height' method where one keeps the distance between the tip and the surface constant thereby observes changes in the tunneling current with the applied voltage.

For a system with very low temperature and small voltages applied in the tunneling current loop one can apply perturbation theory to compute the tunneling current in terms of the unperturbed tip and surface states. According to Fermi's golden rule, the current at position $\mathbf{r}$ and STM bias voltage V is (the formula given here can be found in [9])

$$I(\mathbf{r}) = \frac{2\pi e}{\hbar} \sum_{t,\nu} |M_{t,\nu}(\mathbf{r})|^2 f(\epsilon_t)[1 - f(\epsilon_\nu)]\delta(\epsilon_t + eV - \epsilon_\nu), \qquad (1.8)$$

where e is the charge of the electron, $t(\nu)$ is the tip(surface) states, f is the Fermi function and $M_{t,\nu}(\mathbf{r})$ is the matrix element from the tip to the surface state at $\mathbf{r}$. The above equation illustrates that the tunneling current is proportional to the square of the matrix element between an occupied tip state and an empty surface state times a factor which gives the probability that the tip state is occupied and the surface state is empty. If one treats the tip as a point source then he/she gets $|M_{t,\nu}(\mathbf{r})|^2 \propto |\psi_\nu(\mathbf{r})|^2$ where $\psi_\nu(\mathbf{r})$ are the eigenfunctions of the surface. At very low temperatures (~ 10 K) one may substitute the Fermi functions by step functions and therefore use the relation $\int d\omega \delta(\epsilon_t + eV - \omega)\delta(\omega - \epsilon_\nu) = \delta(\epsilon_t + eV - \epsilon_\nu)$ to get

$$I(\mathbf{r}) = \frac{2\pi e}{\hbar} \sum_{t,\nu} \varrho_t(\epsilon)|\psi_\nu(\mathbf{r})|^2\delta(\epsilon - E_\nu). \qquad (1.9)$$

where $\varrho_t(\epsilon)$ is the density of states of the tip states. In Eq. 1.9 $\sum_\nu |\psi_\nu(\mathbf{r})|^2\delta(\epsilon - E_\nu)$ is the local density of states of the surface states at position $\mathbf{r}$ and energy ϵ. Therefore replacing the sum over tip states by an integral one can write

$$I(\mathbf{r}) \propto \int_0^{eV} \varrho_t(\epsilon) LDOS(\mathbf{r}, \epsilon) d\epsilon. \qquad (1.10)$$

Assuming $\varrho_t(\epsilon)$ is constant one gets,

$$I(\mathbf{r}) \propto \int_0^{eV} LDOS(\mathbf{r}, \epsilon) d\epsilon, \qquad (1.11)$$

and

$$\frac{dI}{dV} \propto LDOS(\mathbf{r}, \epsilon). \qquad (1.12)$$

The above calculation is one of the ways to interpret STM dI/dV data that relates it to the LDOS of the surface states.

1.3 Spectroscopic observation of the Kondo resonance

Madhavan *et al* [7] first reported the measurement of local electronic structure of an isolated Kondo impurity on a metallic surface. STM was used to obtain spectroscopic data on individual Co atoms deposited onto Au(111) surface at 4K. Fig. 2 and Fig. 3 of [7] shows the differential conductance dI/dV spectra measured (Fig. 2) without and with a Co atom on Au(111) surface and (Fig. 3) with the STM tip held at various distances from the center of the Co atom. It clearly shows a sharp suppression in the differential conductance dI/dV near the Fermi energy when the STM tip is in the immediate vicinity of the magnetic impurity.

The Kondo resonance has also been observed by Li *et al* [6] for the system of a single Ce impurity on Ag(111) surface at 5K. Fig. 1 and 2 [6] shows the presence of Kondo resonance on Ce adatom atom which is absent for nonmagnetic Ag adatoms.

Manoharan *et al* [1] reported observing the same sharp dip near the Fermi energy in the dI/dV spectra at the location of Co adatom on Cu(111) surface as shown in Fig. 1 of [1]. Knorr *et al* [8] also observe a Kondo resonance for Co adatoms on Cu(111) surface (Fig. 2 of [8]) and the effect of surface state on the dI/dV spectra. The dip observed in the various experimetns just mentioned has been interpreted as a Kondo resonance. Madhavan *et al* [7] have done a detailed comparison of the experimental dip with the expected theoretical dip that one can expect due to Kondo effect. The explanation behind measuring the Kondo resonance as a dip in the dI/dV spectra and how good the experimental results fit with theory are the topics of Sec. 1.5. It should be noted that among the large number of experiments performed on similar systems and conditions we have mentioned only the relevant ones for this particular work.

1.4 The quantum mirage experiment

A very interesting property of a surface is that it can introduce energy levels in the crystal band gaps (often known as surface states). This is because the wave functions do not obey Bloch's theorem in the direction perpendicular to the surface and can decay exponentially away from the surface towards both the bulk material and the vacuum. Therefore electrons are free to move in the plane of the surface which forms a type of two-dimensional electron gas there. Often, the surface-state band is only partially filled, giving a low density on the surface, and a nearly quadratic dispersion relation with a constant effective mass. In case of the Cu(111) surface the electrons in the quasi two-dimensional electron gas belong to the surface state band with an energy minimum at 0.45 eV below Fermi energy [18]. Now, it is well known that the presence of defects in a metal like Cu will introduce charge screening that has an oscillatory component known as *Friedel oscillations* [23]:

$$\phi(\mathbf{r}) = \frac{1}{r^3} cos(2k_F r).$$

Crommie *et al* [10] reported confining the surface electrons by using a closed structure (corrals) built from iron adatom on Cu(111) surface. Their STM topographic image of a circular electronic resonator constructed with Fe adatoms on Cu(111) surface shows beautiful standing wave pattern (Fig. 2 of [10]) which are interpreted as the Friedel type of charge oscillations.

Manoharan used the same idea of confined electrons but in an elliptical corral instead of a circular one and then use it to project the Kondo resonance. They first used a scanning tunneling microscope (STM) to position cobalt atoms in an elliptical ring, and then placed another cobalt atom at one of the two focal points of the ring. Now, while a circle has only one center an ellipse has two 'focal points' or foci. Just like in an elliptical room where a faint sound generated at either of the two foci can be heard clearly far across the chamber at the other foci Manoharan *et al* used a quantum state that concentrated large electron densities at each focus point of the elliptical corral. When they placed a cobalt atom at one focus, a mirage appeared at the other focus: the same electronic states in the surface electrons surrounding the cobalt atom were detected on the other foci by the spectroscopic measurement of STM even though no magnetic atom was actually there. In other words, in the dI/dV spectra the same resonance line shape, width and zero-bias shift were detected on the empty foci as produced by the real atom only attenuated by a factor of about eight.

1.5 Current theoretical interpretation of STM results

In the STM experiments on metallic surfaces with magnetic impurities [1, 6, 7] one observes a dip in the dI/dV spectra at Fermi energy. This dip has been interpreted as a Kondo resonance exhibiting a Fano profile. To explain this observation it is important to note that, in systems like these, below T_K, there exists a roughly Lorentzian shaped LDOS of the 3d orbital near E_F. There is also a conduction electron LDOS of the substrate due to the Abrikosov- Shul resonance discussed in Sec. 1.1. The width of the resonance, ΔE, is proportional to the Kondo temperature, $\Delta E \propto k_B T_K$. Madhavan *et al* [7] pointed out that for a tunneling experiment into the resonance, one should expect dI/dV to reflect the d orbital spectral density and reveal a Lorentzian like peak about E_F. But this can only happen when one assumes that electrons can only tunnel into the d orbital of a magnetic impurity and ignores electron tunnel into the surrounding continuum of conduction band states. This situation is far away from reality where an electron tunneling form a STM tip to the Kondo resonance has two possible channels, i.e., d orbital and the continuum, and this leads to an additional quantum interference term. Effect of such interference for transitions from an arbitrary initial state to a noninteracting discrete state in resonance with a continuum has been calculated by Fano [12]. The dI/dV spectra that has a Fano line shape varies with the lateral tip-adatom distance r as shown in Fig. 2 of [8].

At this point we want to illustrate the theory of this line shape which has been developed by Fano [12]. Let us consider an atomic system containing one discrete state ϕ and a continuum of states ψ_E. Each of these states is non-degenerate. For such a composite system let the final state to be Ψ_E. The ratio of the transition probability from any initial state i through any transition operator T to the final state Ψ_E and the transition probability from i to the initial unperturbed continuum state ψ_E can be represented by a single family of curves. These curves are represented by

$$\frac{|\langle \Psi_E|T|i\rangle|^2}{|\langle \psi_E|T|i\rangle|^2} = \frac{(q+\epsilon)^2}{1+\epsilon^2} = 1 + \frac{q^2 - 1 + 2q\epsilon}{1+\epsilon^2} \tag{1.13}$$

where q is the so called Fano line shape parameter and ϵ is an energy variable. According to Plihal and Gadzuk [15] the tunneling conductance can be written as

$$\frac{dI}{dV}(r, V) = c + a(r)\frac{q(r)^2 - 1 + 2q(r)\epsilon}{\epsilon^2 + 1} \tag{1.14}$$

where $\epsilon = (eV + \Delta E)/(k_B T_K)$, c is the background dI/dV signal and ΔE is the small shift of the resonance from the Fermi energy [8]. The Fano line shape parameter $q(r)$ is given by

$$q(r) = \frac{\text{Re}G(r) + t(r)}{\text{Im}G(r)} \qquad (1.15)$$

where $G(r)$ is the modified conduction electron Green's function as seen by the tip and $t(r)$ is a function proportional to the matrix element for direct tunneling into the localized state. $t(r)$ depends on the overlap of the tip wave function with the localized state and it falls off rapidly with r following the relation $t(r) = t_0 \exp[-d(r)/\alpha]$ where $d(r)$ is the tip-adatom distance and α is the decay length. Fig. 1 of [12] shows line shapes for different values of q. From Eq. 1.15 one can see that even for no direct tunneling to the localized state i.e., when $t = 0$, a Fano line shape can result due to the indirect tunneling from the tip to the adsorbate by conduction electron propagation represented by $\text{Re}G(r)/\text{Im}G(r)$. Knorr *et al* [8] reported for an on-atom ($r = 0$) position of the tip from the fitting of the measured $dI/dV(V)$ curves that the Kondo temperature T_K for Co/Cu(111) is (54 ± 2)K and the value of the Fano parameter $q = 0.18 \pm 0.03$. Manoharan *et al* [1] reported a similar value of $T_K = (53 \pm 5)$K of for the Co/Cu(111) adatom-substrate system.

This line shape is also detectable only for $r < 10$ Å. Hence the dip seen in the STM experiments are interpreted as the Kondo resonance [14] showing up as Fano resonance [12] that has a width that determines the Kondo temperature.

Gunnarsson *et al* [25] tried to interpret the experimental line shape by neglecting the direct coupling between the tip and the adsorbate $3d$ orbital and with the substrate d orbital. Jones-Jennings-Jepsen potential is used for the surface wave function and the adsorbate is modeled by a single d orbital and the momentum dependence of the hybridization matrix elements is considered explicitly. Results from the study matched quite well with the experimental data even when the surface states are not included in the calculation.

1.6 Problems with the interpretation of STM results

After specifying the features of the 'quantum mirage' experiment we address the unanswered questions that arise from it. One crucial issue is that once one knows how to get Kondo Hamiltonian then he/she can solve it for spin $S = 1/2$ systems. In Co we have 5 d orbitals (some of them are degenerate) with the number of electrons yet to be fixed for Co adatoms embedded in Cu(111) surface. Therefore this problem of Co adatom is much more complicated and it is not clear what kind of model Hamiltonian one should use in this case.

In the above discussion we have always assumed that there is only one kind of substrate state that can be tunneled to. But the eigenstates of the substrate can be linear combination of atomic states with coefficients that are strongly energy depen-

dent. This is why, in general, the matrix elements for tunneling from the tip to the various atomic basis states can be very different because the tunneling matrix elements are strongly energy dependent. For example for Co on top of Cu the tunneling to atomic d states will have smaller matrix elements than that to the more extended p and s states . Also because of the broken symmetry at the surface the p and s states mix with the d states and we have in general a very complicated problem. However the interpretation of the tunneling experiments is generally done with the assumption that Eq.s 1.11 and 1.12 are correct.

Because the resonance at Fermi energy depends on temperature these experimental results are interpreted with the help of Kondo physics. Kondo cloud is related to Kondo temperature which is determined by the width of the resonance at E_F. Fano line shape is detected only within the range $r < 10$ Åwhere r is the lateral distance between the tip and adatom. But Kondo temperature estimated from the experiments are $\sim 50K$ corresponds to a much bigger Kondo cloud compare to 10 Åat least if we use a simple interpretation that the energy scale determined by the width would tell us what the range of states at the Fermi energy is that are involved. This would result in only a small number of k states and therefore a large cloud radius.

In the interpretation of dI/dV spectra as a quantity proportional to LDOS one assumes the STM tip as a point source (represented by s orbital) with constant density of states. But this might not be the case and the orbitals present at the tip might be playing an important role as the tunneling current is proportional to the tunneling matrix element from the tip to the surface.

From Eq. 1.15 one can see that Fano parameter depends on the lateral distance between the tip and adatom. Therefore a change in this distance will change the value of q which therefore expect to result in the dI/dV spectra. But no such change in the dI/dV spectra is noticed as one can see from Fig. 2 of [7].

Since T_K has a very sensitive dependence on electron density at a certain site we expect a variation of T_K if the Co adatom is placed near a step edge. But experiments [16, 22] did not found any dependence of T_K on the position of Co adatom on Cu(111), Ag(111) or Au(111).

1.7 Motivation for the ab-initio study

As mentioned in the previous section that dI/dV measures local density of states (LDOS) times the tunneling matrix element squared, it is important to know the possible tunneling states present near the vicinity of STM tip in real space. We also mentioned that the total scattering cross section of the conduction electrons scattered by the impurity localized states is proportional to its (localized state) LDOS. Therefore one needs to know the electronic distribution of this Co adatom on Cu(111) surface system. Also one wants to know the form of an effective hamiltonian for the system with numerical values for most important hopping parameters. To explain ex-

perimental observations such as the width of Kondo resonance near Fermi energy, one must know the coupling between different states of the system. Prerequisite condition for that is to know the local density of states near Fermi energy. Therefore we want to study the electronic structure of Co adatom on Cu(111) surface. Density functional theory (DFT) is one of the most efficient and accurate method for calculating the ground state electronic properties of a system of interacting electrons. Within DFT methods one can calculate different physical properties of the system with high level of accuracy. Therefore we treat this problem in hand with DFT method.

The rest of the thesis is organized as follows: Chapter 2 gives a very brief introduction to our main tool of investigation, namely the density functional theory. Results of our study are given in chapters 3 and 4 and they form the heart of the thesis. In chapters 3 and 4 we wanted to simulate the system of our interest, a single Co adatom on Cu(111) surface. Chapter 3 only deals with how to make a slab made of Cu(111) plane that effectively simulates the substrate used in the STM experiments. In chapter 4 we placed Co atoms on top of the slab and studied the electronic structure of Co. The results are discussed in chapter 5.

Chapter 2

Density Functional methods

Density functional theory (DFT) is one of the most successful approaches to quantum mechanical many-body electronic structure calculations of molecular and condensed matter systems. It is essentially a variational method whose success not only encompasses standard bulk materials but also complex materials such as proteins and carbon nanotubes.

Traditional methods for calculating electronic structure of a system of interacting electrons, like Hartree-Fock theory are based on the complicated many-electron wave function. The main objective of the density functional theory is to replace the many-body electronic wave function with the ground state electronic density as the basic quantity. DFT is, therefore, derived from the N-particle Schrödinger equation and is entirely expressed in terms of the density distribution of the ground state, $\rho_{GS}(\mathbf{r})$, and the single particle wave function ϕ_j. Whereas the many-body wave function is dependent on 3N variables, three spatial variables for each of the N electrons, the density is only a function of three variables and is a simpler quantity to deal with both conceptually and practically, i.e. DFT reduces the calculations of the ground state properties of systems of interacting particles exactly to the solution of single-particle Hartree-type equations. This is why it has been most useful for systems of very many electrons and therefore we decided to use DFT methods for calculating the electronic structure of a cobalt adatom on copper (111) surface. In particular, we used two powerful approximation methods such as Linear Muffin Tin Orbital approximation (LMTO) and Linear Augmented Plane Wave method (LAPW) to do our calculations. The LAPW program has the name WIEN2k and the method is also known as the Full Potential Method. In this chapter we briefly discuss the formulation of DFT and important features of LMTO and full potential methods.

2.1 Thomas-Fermi theory for electron density

One can start from Thomas-Fermi theory that says for interacting electrons moving in an external potential $v(\mathbf{r})$ due to the ion cores, the relation between $v(\mathbf{r})$ and the

density distribution $\rho(\mathbf{r})$ is:

$$\rho(\mathbf{r}) = \gamma(\mu - v_{eff}(\mathbf{r}))^{3/2} \tag{2.1}$$

$$v_{eff}(\mathbf{r}) \equiv v(\mathbf{r}) + \int \frac{\rho(\mathbf{r}')}{|\mathbf{r} - \mathbf{r}'|} d\mathbf{r}' \tag{2.2}$$

where $\gamma = \frac{1}{3\pi^2} \left(\frac{2m}{\hbar^2}\right)^{3/2}$ and μ is the $\mathbf{r}$ independent chemical potential. The second term in Eq. 2.2 is the classical electrostatic potential generated by the density $\rho(\mathbf{r})$ of all the valence electrons. Eq. 2.1 works best for systems of slowly varying density [26, 27].

2.2 The first Hohenberg-Kohn theorem

Hohenberg and Kohn started from Thomas-Fermi theory and establish the connection between the electron density and the many-electron Schrödinger equation (which is expressed in terms of $\psi(\mathbf{r_1}, \mathbf{r_2}, .., \mathbf{r_N})$).

We start with Hohenberg-Kohn theorems which are at the heart of the density functional theory.

The first Hohenberg-Kohn theorem states that

The ground state density $\rho_{GS}(\mathbf{r})$ of a bound system of interacting electrons in some external potential $v(\mathbf{r})$ determines this potential uniquely [28],[29].

Proof: This proof is valid for a non-degenerate ground state. Let $\rho_{GS}(\mathbf{r})$ be a non-degenerate ground state density of N electrons in the potential $v_1(\mathbf{r})$ corresponding to the ground state ψ_1 and the energy E_1. Then

$$E_1 = \langle \psi_1 | H_1 | \psi_1 \rangle = \int v_1(\mathbf{r}) \rho_{GS}(\mathbf{r}) d\mathbf{r} + \langle \psi_1 | T + V_{ee} | \psi_1 \rangle \tag{2.3}$$

where H_1 is the total Hamiltonian corresponding to v_1, T and V_{ee} are the kinetic and interaction energy operators for the electrons. Now one can assume that there exists a second potential $v_2(\mathbf{r})$, not equal to $v_1(\mathbf{r})$ + constant, with ground state ψ_2, necessarily $\psi_2 \neq e^{i\theta}\psi_1$ which gives rise to the same $\rho_{GS}(\mathbf{r})$. Thus

$$E_2 = \langle \psi_2 | H_2 | \psi_2 \rangle = \int v_2(\mathbf{r}) \rho_{GS}(\mathbf{r}) d\mathbf{r} + \langle \psi_2 | T + V_{ee} | \psi_2 \rangle \tag{2.4}$$

Since ψ is assumed to be non-degenerate, the Rayleigh-Ritz minimal principle gives

$$E_1 < \langle \psi_2 | H_1 | \psi_2 \rangle \quad = \int v_1(\mathbf{r}) \rho_{GS}(\mathbf{r}) d\mathbf{r} + \langle \psi_2 | T + V_{ee} | \psi_2 \rangle$$

$$= E_2 + \int (v_1(\mathbf{r}) - v_2(\mathbf{r})) \rho_{GS}(\mathbf{r}) d\mathbf{r} \qquad (2.5)$$

$$E_2 < \langle \psi_1 | H_2 | \psi_1 \rangle \quad = \int v_2(\mathbf{r}) \rho_{GS}(\mathbf{r}) d\mathbf{r} + \langle \psi_1 | T + V_{ee} | \psi_1 \rangle$$

$$= E_1 + \int (v_2(\mathbf{r}) - v_1(\mathbf{r})) \rho_{GS}(\mathbf{r}) d\mathbf{r} \qquad (2.6)$$

Addition of Eq. 2.5 and 2.6 leads to the contradiction.

$$E_1 + E_2 < E_1 + E_2.$$

Therefore it is proved that the existence of a second potential which is not equal to $v_1(\mathbf{r})$ + constant and gives the same $\rho_{GS}(\mathbf{r})$ must be wrong.

Also, $\rho_{GS}(\mathbf{r})$ determines the number of electrons, N

$$N = \int \rho_{GS}(\mathbf{r}) d\mathbf{r}. \qquad (2.7)$$

Since $\rho_{GS}(\mathbf{r})$ determines both N and $v(\mathbf{r})$, it gives the full hamiltonian and all properties derivable from the hamiltonian through the solution of time independent or time dependent Schrödinger equation (even in the presence of the additional perturbation like electromagnetic fields). For example, the many body eigenstates $\psi^0(\mathbf{r_1}, \mathbf{r_2}, ..., \mathbf{r_N})$, $\psi^1(\mathbf{r_1}, \mathbf{r_2}, ..., \mathbf{r_N})$,..., the 2 particle Green's function $G(\mathbf{r_1}, t_1; \mathbf{r_2}, t_2)$ and so on. This theory is extended later in the case of degenerate ground state[30] and is also valid for the special case of non interacting electrons.

2.3 The second Hohenberg-Kohn theorem

The most important property of an electronic ground state is its energy E_{GS}. One can calculate it by variational principle:

$$E_{GS} = min_\psi \langle \psi | H | \psi \rangle \qquad (2.8)$$

Hohenberg and Kohn expressed the minimum energy using density. The derivation given below follow the steps of R.O. Jones[33] (but Levy[31] and Lieb[32] first showed the derivation in this way which is simpler than the original derivation by Hohenberg and Kohn). One considers N electrons moving in an external potential $v_{ext}(\mathbf{r})$, i.e., the hamiltonian is

$$H = T + V_{ee} + \sum_{i=1}^{N} v_{ext}(\mathbf{r_i}), \tag{2.9}$$

where H and V_{ee} are the kinetic and electron-electron interaction operators respectively. Now Levy defined a universal functional (since the functional does not refer to any specific system and any specific potential)

$$F[\rho] = min_{\psi \to \rho} \langle \psi | T + V_{ee} | \psi \rangle, \tag{2.10}$$

or

$$F[\rho] = \langle \psi_{min}^{\rho} | T + V_{ee} | \psi_{min}^{\rho} \rangle \tag{2.11}$$

where the minimum is taken over all ψ that give ρ. The density ρ at any position $\mathbf{r_1}$ is defined to be

$$\rho(\mathbf{r_1}) = N \int d\mathbf{r_2} ... \int d\mathbf{r_N} \psi^*(\mathbf{r_1}, \mathbf{r_2}, ..., \mathbf{r_N}) \psi(\mathbf{r_1}, \mathbf{r_2}, ..., \mathbf{r_N}). \tag{2.12}$$

The second Hohenberg-Kohn theorem states

$$E[\rho] \equiv \int d\mathbf{r} v_{ext}(\mathbf{r}) \rho(\mathbf{r}) + F[\rho] \geq E_{GS}, \tag{2.13}$$

and

$$\int d\mathbf{r} v_{ext}(\mathbf{r}) \rho_{GS}(\mathbf{r}) + F[\rho_{GS}] = E_{GS}. \tag{2.14}$$

Proof: Writing $v = \sum_{i=1}^{N} v_{ext}(\mathbf{r_i})$ one gets

$$\int d\mathbf{r} v_{ext}(\mathbf{r}) \rho(\mathbf{r}) + F[\rho] = \langle \psi_{min}^{\rho} | v + T + V_{ee} | \psi_{min}^{\rho} \rangle \geq E_{GS}, \tag{2.15}$$

according to the minimum property of the ground state. Use of the minimum property once more gives

$$E_{GS} = \langle \psi_{GS} | v + T + V_{ee} | \psi_{GS} \rangle \leq \langle \psi_{min}^{\rho_{GS}} | v + T + V_{ee} | \psi_{min}^{\rho_{GS}} \rangle. \tag{2.16}$$

Now subtracting the interaction with the external potential gives

$$\langle \psi_{GS} | T + V_{ee} | \psi_{GS} \rangle \leq \langle \psi_{min}^{\rho_{GS}} | T + V_{ee} | \psi_{min}^{\rho_{GS}} \rangle. \tag{2.17}$$

The above equation is true only when

$$\langle \psi_{GS} | T + V_{ee} | \psi_{GS} \rangle = \langle \psi_{min}^{\rho_{GS}} | T + V_{ee} | \psi_{min}^{\rho_{GS}} \rangle. \tag{2.18}$$

Then one has

$$
\begin{aligned}
E_{GS} &= \int d\mathbf{r}\, v_{ext}(\mathbf{r})\rho_{GS}(\mathbf{r}) + \langle\psi_{GS}|T + V_{ee}|\psi_{GS}\rangle \\
&= \int d\mathbf{r}\, v_{ext}(\mathbf{r})\rho_{GS}(\mathbf{r}) + \langle\psi_{min}^{\rho_{GS}}|T + V_{ee}|\psi_{min}^{\rho_{GS}}\rangle \\
&= \int d\mathbf{r}\, v_{ext}(\mathbf{r})\rho_{GS}(\mathbf{r}) + F[\rho_{GS}].
\end{aligned}
\tag{2.19}
$$

Hence the second Hohenberg-Kohn theorem is proved. It follows from Eq. 2.18 that if the ground state is non-degenerate, $\psi_{min}^{\rho_{GS}} = \psi_{GS}$. If the ground state is degenerate $\psi_{min}^{\rho_{GS}}$ is equal to one of the ground state wave functions, and the others can also be obtained. The ground state density then determines the ground state wave function(s), from which all ground state properties can be calculated. These properties are therefore functionals of the density which the Hohenberg-Kohn theorem has stated before. But these theorems do not specify the form of the functional dependence of energy on the density. Hohenberg and Kohn only states that to get back to the Thomas-Fermi theory, $\langle V_{ee}\rangle$ with respect to the ground state can be written as

$$
\langle\psi_{GS}|V_{ee}|\psi_{GS}\rangle = \frac{1}{2}\int d\mathbf{r}d\mathbf{r}' \frac{\rho_{GS}(\mathbf{r})\rho_{GS}(\mathbf{r}')}{|\mathbf{r} - \mathbf{r}'|}.
\tag{2.20}
$$

However they did not give the density representation of the kinetic energy part of the electrons. At this point Kohn-Sham gives a set of single particle equations which largely remedied the problem involving the form of kinetic energy and is the next major step in the development of DFT.

2.4 The self-consistent Kohn-Sham equations

Kohn-sham self-consistent equations are very similar to the Hartree self-consistent single particle equations for the approximate description of the electronic structure of atoms (Hartree equations are based on Thomas-Fermi theory where every electron is regarded as moving in an effective potential generated by the average charge density of all the other electrons). Hartree equations are the following

$$\left\{ -\frac{1}{2}\nabla^2 + v_H(\mathbf{r}) \right\} \phi_j(\mathbf{r}) = E_j \phi_j(\mathbf{r}) \qquad (2.21)$$

$$\rho(\mathbf{r}) = \sum_{j=1}^{N} |\phi_j(\mathbf{r})|^2 \qquad (2.22)$$

$$v_H(\mathbf{r}) = -\frac{Z}{\mathbf{r}} + \int d\mathbf{r}' \frac{\rho(\mathbf{r}')}{|\mathbf{r} - \mathbf{r}'|} \qquad (2.23)$$

where in Eq. 2.21 j denotes both spatial and spin quantum numbers, $\rho(\mathbf{r})$ in Eq. 2.22 is the mean density (for which, in the ground state, the sum runs over N lowest eigenvalues) and $v_H(\mathbf{r})$ in Eq. 2.23 is the effective single particle potential. In the expression for $v_H(\mathbf{r})$ the first term represents the potential due to a nucleus of atomic number Z and the second term represents the potential due to the average density distribution $\rho(\mathbf{r})$.

To solve these equations one may start from a first approximation (e.g., Thomas-Fermi theory), construct $v_H(\mathbf{r})$, solve Eq. 2.21 and recalculate $\rho(\mathbf{r})$ from Eq. 2.22, which should be the same as the initial $\rho(\mathbf{r})$. If it is not one iterates appropriately until it is.

The Hartree differential Eq. 2.21 takes the form of the *Schrödinger* equation for non-interacting electrons moving in the external potential v_{eff}. So for such a system the HK variational principle becomes

$$E_{v(\mathbf{r})}[\rho] \equiv \int d\mathbf{r} v(\mathbf{r})\rho(\mathbf{r}) + T[\rho(\mathbf{r})] \geq E_{GS}, \qquad (2.24)$$

where $T[\rho(\mathbf{r})]$ is the kinetic energy of the ground state of non-interacting electrons with density distribution $\rho(\mathbf{r})$. One wants Eq. 2.22 to be stationary with respect to the variations of $\rho(\mathbf{r})$ which leave the total number of electrons unchanged, and the Euler-lagrange equation for this purpose is

$$\delta E_v[\rho(\mathbf{r})] \equiv \int \delta\rho(\mathbf{r}) \left\{ v(\mathbf{r}) + \frac{\delta T[\rho(\mathbf{r})]}{\delta\rho(\mathbf{r})}|_{\rho=\rho_{GS}} - \epsilon \right\} d\mathbf{r} = 0, \qquad (2.25)$$

where ρ_{GS} is the exact ground state density for $v(\mathbf{r})$ and ϵ is a Lagrange multiplier to assure particle conservation. In this case the ground state energy and density can be obtained by solving the single particle equations

$$\left(-\frac{1}{2}\nabla^2 + v(\mathbf{r}) - E_j\right)\phi_j(\mathbf{r}) = 0 \tag{2.26}$$

$$\rho_{GS}(\mathbf{r}) = \sum_{j=1}^{N} |\phi_j(\mathbf{r})|^2 \tag{2.27}$$

$$E_{GS} = \sum_j E_j. \tag{2.28}$$

To match this description with the case of interacting electrons Kohn-Sham write the functional $F[\rho(\mathbf{r})]$ in the following form

$$F[\rho(\mathbf{r})] \equiv T[\rho(\mathbf{r})] + \frac{1}{2}\int d\mathbf{r}d\mathbf{r}'\frac{\rho(\mathbf{r})\rho(\mathbf{r}')}{|\mathbf{r}-\mathbf{r}'|} + E_{xc}[\rho(\mathbf{r})], \tag{2.29}$$

where $E_{xc}[\rho(\mathbf{r})]$ is the so called exchange-correlation energy functional. The HK variational principle for interacting electrons is therefore

$$E_{v(\mathbf{r})}[\rho] \equiv \int d\mathbf{r}v(\mathbf{r})\rho(\mathbf{r}) + T[\rho(\mathbf{r})] + \frac{1}{2}\int d\mathbf{r}d\mathbf{r}'\frac{\rho(\mathbf{r})\rho(\mathbf{r}')}{|\mathbf{r}-\mathbf{r}'|} + E_{xc}[\rho(\mathbf{r})] \geq E_{GS}. \tag{2.30}$$

The corresponding Euler-lagrange equation is

$$\begin{aligned}\delta E_v[\rho(\mathbf{r})] &\equiv \int \delta\rho(\mathbf{r})\left\{v(\mathbf{r}) + \frac{\delta T[\rho(\mathbf{r})]}{\delta\rho(\mathbf{r})}\Big|_{\rho=\rho_{GS}}\right. \\ &\quad + \left.\int d\mathbf{r}'\frac{\rho(\mathbf{r}')}{|\mathbf{r}-\mathbf{r}'|} + \frac{\delta E_{xc}[\rho(\mathbf{r})]}{\delta\rho(\mathbf{r})}\Big|_{\rho=\rho_{GS}} - \epsilon\right\}dr = 0. \end{aligned}\tag{2.31}$$

Now let one write

$$v_{xc}(\mathbf{r}) \equiv \frac{\delta E_{xc}[\rho(\mathbf{r})]}{\delta\rho(\mathbf{r})}\Big|_{\rho=\rho_{GS}} \tag{2.32}$$

and

$$v_{eff}(\mathbf{r}) \equiv v(\mathbf{r}) + \int d\mathbf{r}'\frac{\rho_{GS}(\mathbf{r}')}{|\mathbf{r}-\mathbf{r}'|} + v_{xc}(\mathbf{r}). \tag{2.33}$$

Substituting these expressions in Eq. 2.31 one finds that it has the same form as Eq. 2.25 for non-interacting particles moving in an effective external potential $v_{eff}(\mathbf{r})$. Therefore the minimizing density $\rho_{GS}(\mathbf{r})$ can be found by solving the single particle equation

$$\left(-\frac{1}{2}\nabla^2 + v_{eff}(\mathbf{r}) - E_j\right)\phi_j(\mathbf{r}) = 0 \tag{2.34}$$

with

$$\rho_{GS}(\mathbf{r}) = \sum_{j=1}^{N} |\phi_j(\mathbf{r})|^2 \tag{2.35}$$

$$E_{GS} = \sum_j E_j + E_{xc}[\rho_{GS}(\mathbf{r})] - \int d\mathbf{r}\, v_{xc}(\mathbf{r})\rho_{GS}(\mathbf{r}) - \frac{1}{2}\int d\mathbf{r}d\mathbf{r}' \frac{\rho_{GS}(\mathbf{r})\rho_{GS}(\mathbf{r}')}{|\mathbf{r} - \mathbf{r}'|}. \tag{2.36}$$

These are the so called Kohn-Sham self consistent equations. If one neglects E_{xc} and v_{xc} altogether, the KS equations (2.34)-(2.36) reduce to the self consistent Hartree equations.

Again to solve these KS equations self consistently one can start with a guess of the charge density ρ_{GS}. By using some approximate form for the functional dependence of E_{xc} on density, one must compute V_{xc} as a function of $\mathbf{r}$. The set of KS equations are then solved to obtain an initial set of KS orbital. This set of orbital is used to compute an improved density from Eq. 2.35 and the process is repeated until the density and exchange correlation energy converge to within some tolerance. After getting the self consistent density, the electronic energy can be computed from Eq. 2.36.

The KS orbital on each iteration can be computed numerically or they can be expressed in terms of a set of basis functions. Therefore by solving the KS equation one can find the coefficients in the basis set expansion. The choice of these basis sets comes with experience.

2.5 Local density approximation

Several different schemes have been developed for obtaining approximate forms for the functional for the exchange correlation energy. The main source of error in DFT usually arises from the approximate nature of E_{xc}. The most widely used and most simple approximation for E_{xc} is the local density approximation (LDA) in which

$$E_{xc}^{LD} = \int \rho_{GS}(\mathbf{r})\epsilon_{xc}[\rho_{GS}(\mathbf{r})]d\mathbf{r} \tag{2.37}$$

where $\epsilon_{xc}[\rho_{GS}(\mathbf{r})]$ is the exchange-correlation energy per electron in a homogeneous electron gas of constant density.

Also for spin polarized systems the local spin density approximation (LSDA) ap-

pears to be the most accurate scheme for DFT calculations. In such a case E_{xc} is given by

$$E_{xc}^{LSD} = \int \rho_{GS}(\mathbf{r})\epsilon_{xc}[\rho_{GS,\uparrow}(\mathbf{r}), \rho_{GS,\downarrow}(\mathbf{r})]d\mathbf{r} \qquad (2.38)$$

where $\epsilon_{xc}[\rho_{GS,\uparrow}(\mathbf{r}), \rho_{GS,\downarrow}(\mathbf{r})]$ is the exchange-correlation energy per particle in a homogeneous, spin -polarized electron gas with spin-up and spin-down densities $\rho_{GS,\uparrow}(\mathbf{r})$ and $\rho_{GS,\downarrow}(\mathbf{r})$ respectively.

These expressions for exchange-correlation energies are clearly approximations because neither positive charge nor electronic charge are uniformly distributed in actual systems. To account for the inhomogeneity of the electron density, a nonlocal correlation involving the gradient of $\rho_{GS}(\mathbf{r})$ is often added to the exchange energy (this is the so called generalized gradient approximation(GGA)). There are many other amendments to E_{xc} relative to the system that one wants to solve in practice.

Two standard programs known as Tight binding-Linear muffin tin orbital-Atomic sphere approximation (TB-LMTO-ASA) and Linear augmented plane wave (also known as Full potential method or WIEN2k) are used to calculate electronic properties of the system of Cobalt impurity deposited on metallic Cu(111) surface. These two programs basically solve the Kohn-Sham self consistent equations and determines the band structure, density of states, total energy and so on. Since Co has a net spin in this system, we used LSDA for the DFT calculations within LMTO and full potential methods.

2.6 Tight binding-Linear muffin tin orbital and atomic sphere approximation method

The tight binding-Linear muffin tin orbital method is a specific implementation of density functional theory within the local density approximation (LDA). In this method each atom in the unit cell is replaced by a sphere of volume of a single atomic cell. This is the so called atomic sphere approximation. In a crystal, atomic states feel the corresponding potential together with some additional potentials from the neighboring atoms. Therefore this problem is avoided by considering a constant potential outside the sphere and this is the muffin tin approximation of the atomic potential.

In this program, the Wigner Seitz spheres are considered as atomic spheres. The crystal is divided up into regions inside muffin-tin spheres and an interstitial region. Inside the muffin-tin spheres the energy independent basis functions are constructed from linear combination of the functions $\phi_l(E_\nu, \mathbf{r})$ (solution of the radial Schrödinger equation at the fixed arbitrary energy E_ν) and their energy derivatives $\dot{\phi}_l(E_\nu, \mathbf{r})$. Therefore LMTO method is no longer exact for muffin-tin potential but the error in

energies and wave functions are of fourth and second order in the difference between eigenvalues of the secular equations (secular equations that one gets for using variational principle for Schrödinger's equation with energy independent basis functions) and E_ν. Another important feature of LMTO is that, in the interstitial region, the value of the potential is equal to the energy of the state being considered. Therefore the state has zero kinetic energy in that region which give rise to an additional error of order (Eigenvalue of the secular equation - V_{mtz}), where V_{mtz} is the potential in the interstitial region.

The program considers a set of s, p, d LMTOs per atom. For the system of Co impurity embedded on Cu(111) surface, only s,p and d orbitals are considered for Cu and Co and s and p orbitals for empty spheres within LMTO calculation. Complete description of the theory of TB-LMTO-ASA method can be found in [35] and [36].

2.6.1 Projecting orbital character using Fatband plots

The amplitude of a particular basis function in a given eigenvector present in a particular band of the band structure can be projected and displayed with the help of so called fatband plots. In these plots the amplitude of the projection is represented by a energy and **k** dependent width added to the band structure. The LMTO method expands the wave function in the atomic orbital basis set $\{\chi_i(k)\}$ in the following form:

$$|\psi(k)\rangle = \sum_{i=1,n=1}^{p,N} c_{i,n}(k)|\chi_i(k)\rangle. \tag{2.39}$$

where i is the atomic orbital index and n is the band index. Therefore at certain k point one can plot $|c_{i,n}|^2$ for a specific orbital basis function that gives the amount of that orbital character present in each bands of the band structure picture. This is the so called fatband plotting. Following is a simple example of fatband plotting.

Let us consider 3 atoms having s orbital only sitting in a row. If we consider the nearest neighbor hopping parameter t and the crystal field splitting for the middle atom to be e then the hamiltonian can be written as

$$H = \begin{bmatrix} 0 & t & 0 \\ t & e & t \\ 0 & t & 0 \end{bmatrix}$$

where these 3 s orbital wave functions make the basis set. For $e = -2$ eV and $t = -1$ eV the eigenvalues are

$$E = [-2.73, 0.00, 0.73]$$

and the corresponding eigenvectors are the following

$$\begin{bmatrix} -0.33 & 0.71 & 0.63 \\ -0.89 & 0.00 & -0.46 \\ -0.33 & -0.71 & 0.63 \end{bmatrix}$$

where $i - th$ column represents $i - th$ eigenvector.

Now $c_i^* c_i$ of the 1st basis orbital in these three eigenvectors are

$$0.11, 0.50, 0.39$$

Also $c_i^* c_i$ for the 2nd and 3rd orbital in the eigenvectors are

$$0.79, 0.00, 0.21$$
$$0.11, 0.50, 0.39.$$

In a fat band plot the width of a level in this example represents the amount of selected orbital character in the eigenstate corresponding to that energy. Hence by plotting fatband one can project different orbital characters in each bands.

2.7 Linear augmented plane wave method or Full potential method (WIEN2k)

This program uses the same basis functions defined with respect to a muffin-tin potential inside the atomic sphere as the LMTO program. The difference of this DFT scheme with LMTO is that in the interstitial region the trial wave functions are chosen to be a linear combination of energy independent augmented plane waves. Therefore it is free from the additional error that is present in LMTO for choosing vanishing kinetic energy for the MTOs in the interstitial region. This program is also known as the most accurate method for calculating the total energy of a system. But we can no longer simply project the orbital characters present in a specified band of the band structure because the basis set contains large number of plane waves in the interstitial region. Description of the full potential program can be found in [37].

We shall use both LMTO and WIEN2k programs simultaneously to calculate electronic properties for the system under consideration and then compare results calculated within both methods to interpret the experimental findings.

Chapter 3

Cu Surface Electronic Structure Study

3.1 Cu bulk electronic structure study

To study properties of the adatoms on Cu(111) surface one needs to learn first about the electronic structure of a Cu bulk and (111) surface. Cu bulk has face centered cubic (FCC) lattice and the space group $Fm - 3m$. The Brillouin zone (BZ) corresponding to this lattice is shown in Fig. 3.1. The electronic configuration of Cu atom is $[Ar]4s^2 4p^0 3d^9$. Therefore only Cu $4s$, $4p$ and $3d$ orbitals are relevant for the electronic structure of Cu bulk near Fermi level.

A solid material contains 6.022×10^{23} electrons and ion cores per cm^3, but the three dimensional translational symmetry allows to reduce this problem to just one unit cell. According to the Bloch theorem, the solution of Schrödinger equation of an electron in a periodic potential $V(\mathbf{r+R}) = V(\mathbf{r})$ (where $\mathbf{R}$ is a lattice vector) has the form

$$\Psi_{\mathbf{k}}(\mathbf{r}) = \exp^{i\mathbf{k}\cdot\mathbf{r}} u_{\mathbf{k}}(\mathbf{r}), \tag{3.1}$$

where the function $u_{\mathbf{k}}(\mathbf{r})$ has the same translational symmetry as the lattice,i.e., $u_{\mathbf{k}}(\mathbf{r} + \mathbf{R}) = u_{\mathbf{k}}(\mathbf{r})$. Here the vector $\mathbf{k}$ is called the momentum vector of the electron since $\hbar\mathbf{k}$ is the momentum. Replacing $\Psi_{\mathbf{k}}(\mathbf{r})$ in the Schrödinger equation by the above function we get a wave equation for $u_{\mathbf{k}}(\mathbf{r})$. The eigenfunctions and eigenvalues of this wave equation are explicit functions of $\mathbf{k}$ as well as the energy is now a multi-valued function of $\mathbf{k}$. That is for each value of $\mathbf{k}$, there is a large number of solutions, giving a set of discrete energies $E_{1,\mathbf{k}}, E_{2,\mathbf{k}}, \ldots$ Since these energies depend on $\mathbf{k}$, they vary continuously as $\mathbf{k}$ is varied over its range of values, forming energy bands for each level. Therefore we write energy eigenvalues as $E_{n,\mathbf{k}}$, and refer to the subscript n as band index. Hence in the simple case such as Cu bulk the electronic properties of the infinite crystal are determined solely by the electronic structure within the first BZ.

The electronic structure of Cu bulk calculated along high symmetry lines in the first Brillouin zone is shown in Fig. 3.2. Note that Fermi level is at zero energy. As one can see the agreement between both methods, LMTO and Full potential, in this case is remarkable. The character of eigen functions at given energies is depicted by so-called fatbands calculated within LMTO method. From Fig. 3.3 one can see that
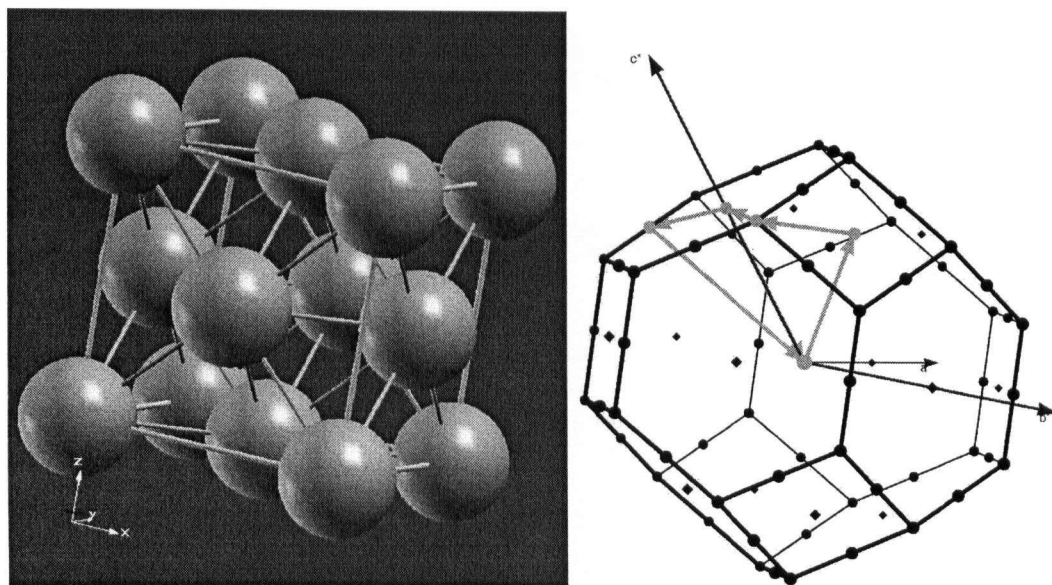
Figure 3.1: Crystal structure of Cu bulk and the corresponding Brillouin zone.

atomic sp orbitals are highly mixed and form almost free electron like bands. However, at the lowest energies (from -10 to -5 eV), these bands bear mostly s character. As the band disperses toward Fermi energy, it gains more and more p character and near the Fermi energy it has mostly $4p$ orbital character. Strong overlap between the s and p orbital wave functions results in such large dispersion for the free electron like band in the band structure. On the other hand the d orbital wave functions are more compact. Therefore direct d-d orbital overlap between neighboring atoms is smaller resulting in only a 4 eV bandwidth for $3d$ bands compare to basically infinite eV for sp bands. In contrast to simple atomic configuration of Cu, the d band of the bulk material is fully occupied resulting in a d^{10} configuration.

3.2 Supercell Calculations and relative error minimizations

To study the electronic structure of the surface one has to brake the periodicity of the lattice at least in one direction. The simplest way is to use a so called supercell approximation.

In the supercell approximation, several neighboring unit cells are combined into one new cell using translation vectors of the original lattice. This 'bigger' unit cell is called a supercell. For example, an FCC crystal can be represented by three FCC
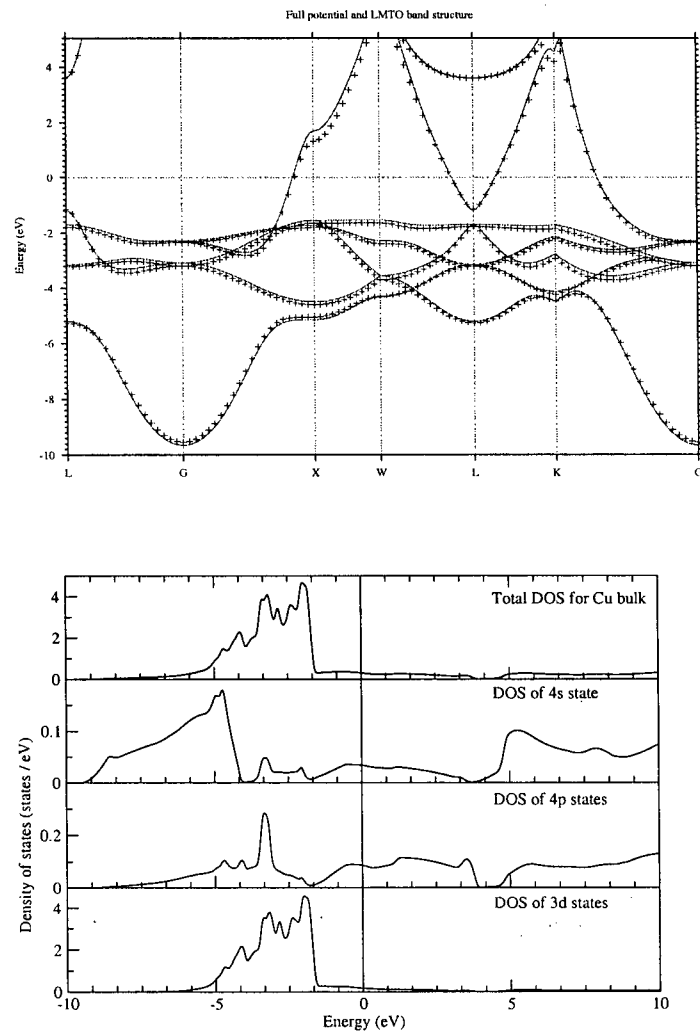
Figure 3.2: Band structure picture for Cu bulk crystal structure from Full potential and LMTO calculation. Lines represents LMTO bands and points represents Full potential bands in the first figure. Density of states (total and partial, calculated within full potential) are shown for Cu bulk in the lower panel. The zero of energy is at Fermi energy.

translation vectors and one atom per unit cell. At the same time it can also be represented by three translation vectors of simple cubic crystal and four atoms per unit cell which is a supercell representation of FCC crystal for the same unit cell. To consider a supercell that combines several unit cells the translation vectors are chosen accordingly. For example, the following choice of the translation vectors for an FCC crystal

$$
\begin{aligned}
a_1 &= 0.0\hat{x} - 0.5\hat{y} + 0.5\hat{z} \\
a_2 &= 0.5\hat{x} - 0.5\hat{y} + 0.0\hat{z} \\
a_3 &= n\hat{x} + n\hat{y} + n\hat{z}
\end{aligned}
\tag{3.2}
$$

(where n is an integer) together with one atom per unit cell represents a supercell that consists of n FCC unit cells in the (111) direction.

This new choice of a larger unit cell is also an approximation because everything is still periodic in the crystal. For example, if one removes one of the four atoms in the FCC supercell (one that is represented by three SC translation vectors together with four atoms per unit cell), one would form a vacancy that will then form a simple cubic lattice in the crystal structure. The same idea is used to simulate vacuum in the crystal structure by removing several adjacent atomic planes. This is often called the slab approximation in which the system is modeled by a sequence like ...|*vacuum*|*Cuslab*|*vacuum*|*Cuslab*|... If we then make the vacuum layer extremely large so that the Cu slabs have virtually no interaction and at the same time make the Cu slabs also infinitely thick the influence of the surfaces at the top and bottom of the cu slabs would give an exact representation of the influence of breaking the translational symmetry at the surface.

In this approximation there are two possible sources of error as far as the properties of the surface are concerned. First type of error arise when the spatial separation between two adjacent slabs is not large enough. In that case the layers of the slabs couple with each other. In the supercell geometry, required for calculations of the surface electronic structure the momentum components parallel to the surface are well defined quantum numbers, whereas the perpendicular component is formally also conserved because our slabs are periodic but for each **k** perpendicular vector now within the very large super cell there would be a large number of bands. The number of bands would be equal to the number of Cu layers in the Cu slab. Within each such band the dispersion in the perpendicular direction will go to zero as the distance between the slabs is increased so they no longer interact. In this limit the state representing these band are discrete and have dispersion only in a direction parallel to the slab. Hence we do not expect to find any continuous dispersion of the energy bands along the direction perpendicular to the surface. But when the slabs are not separated enough, because of the coupling between slabs some dispersion in

band structure along $k_\perp$ is present. The first step in this calculation is to determine the spatial separation between two slabs needed to decouple the surface layers of the adjacent slabs.

The second type of error occurs when the slab is too thin. In contrast to the real material where one has only one surface, in the slab approximation there are two 'physical' surfaces. Therefore in the resulting band structure there will be at least two sets of bands associated with different surfaces. If there is no coupling between them they should be degenerate. On the other hand when the slab is too thin, the two surfaces of the same slab can couple to each other and the degeneracy on the surface states is lifted.

Another effect is the change in the band width as a function of the number of layers in a slab. In a thin slab, atoms do not have all the hopping possibilities between the planes compare to bulk. This significantly reduces the band width for bands with different orbital characters compare to bulk band widths. Therefore it is important to make sure that errors due to slab approximation are minimized before doing any calculation. To do this we simply carry out calculations as a function of the slab thickness and the vacuum layer thickness to determine at which minimum thickness the errors introduced are small enough that they will not influence the physics we are after.

3.3   A single Cu(111) plane

The simplest starting point to understand the electronic structure of Cu(111) surface is to look at the electronic structure of one single layer. Note that a Cu(111) plane has trigonal symmetry as shown in Fig. 3.4. The space group is $P - 3m1$. The corresponding Brillouin zone is shown in Fig. 3.4. We shall show later that in the full potential method a spatial separation of 20.95 a.u. between slabs is sufficient to decouple the layers of different slabs. Hence in the full potential calculation of a single layer, the lattice constant along direction perpendicular to the (111) plane has been taken to be 20.95 a.u.

The slab approximation in LMTO method is introduced by replacing Cu atoms with the empty spheres for the number of layers corresponding to the thickness of the vacuum layer we are trying to simulate. We find that six layers of empty spheres between two Cu(111) planes effectively serves as the vacuum between adjacent slabs in this case. This corresponds to the distance of 26.63 a.u. between Cu layers and is close to what we found for the full potential method. A comparative study of the band structure from LMTO and Wien2k-Full potential methods is shown in Fig. 3.5.

Fig.(3.5) shows that bandwidths of bands bearing characteristics of different orbitals become significantly narrower than compared to bulk Cu. For example, the bandwidth of $3d$ bands is 1.5 eV compare to 4 eV in bulk Cu. This is expected since a single Cu(111) plane is essentially two dimensional and it does not have the

hopping possibilities between the planes compare to Cu bulk. The nearest neighbor coordination number is only 6 as compared to 12 in the bulk FCC structure. Very naively one would guess that the band width would be reduced by about a factor of two.

Because of the symmetry of the Cu(111) plane, the degeneracy of $4p$ orbitals is lifted resulting in different bands bearing different orbital characters of p_x, p_y and p_z. One finds from fatband plots that the band crossing E_F has mostly $p_x + p_y$ (about 60 percent) orbital character and the band at 2 eV above E_F at the Γ point has mostly p_z character.

3.4 Electronic structure as a function of the number of layers

In this section the electronic structure of a Cu(111) slab is studied as a function of the number of layers in the slab. To make the slab, more Cu(111) planes are gradually added to the single Cu(111) plane. The study of important features of the corresponding band structures fixes the number of layers in the slab.

As was discussed in the previous section, for a single layer the band width of $3d$ band gets significantly narrower than that of Cu bulk. The most immediate change to notice from the band structure of three Cu(111) planes is that most of the band width of the $3d$ bands has been restored.

Minimization of the error due to coupling between the layers of two adjacent slabs requires the study of the band structure with different slab separations. Therefore, within full potential method, self consistent band structure calculations have been carried out for several spatial separations between adjacent slabs. The resulting band structures are shown in Fig. 3.7. One can clearly see that for 6.75 a.u. separation between two slabs, bands along the high symmetry line of Γ to A disperses strongly because of the presence of k_z ($k_\perp$ to the surface for this case) dispersion. Upon increasing the spatial separation the bands become less dispersive along this Γ to A line. For a separation of more than 20.95 a.u. there is a negligible dispersion in the band structure along the specified line and the bands are almost completely flat. Hence for this spatial separation slabs are successfully decoupled. One therefore fixes this spatial separation between slabs in all the later calculations by Wien2k-full potential method. In LMTO method the same purpose is served by a spatial separation of 26.63 a.u. between two adjacent slabs.

In the band structure calculated within full potential method for 7 Cu(111) layer slab, Shockley surface states appear in the sp-band gap at Γ point. Because of the presence of two 'physical' surfaces in the simulated crystal structure and the coupling between them, the degeneracy of the two surface states is lifted. Therefore two surface states show up below E_F at Γ point in the band structure. This is a result of choosing

a slab that is not thick enough to decouple the two surfaces of the same slab. Several band structures with different number of layers in the slab are studied in this respect. With the increase of the number of layers in the slab, the decrease in splitting between these two surface states at Γ point is observed. At the same time, together with the increasing number of energy bands, the bandwidths of different bands are restored to that of bulk Cu. Fig. 3.8 shows that in the band structure of a 15 layer slab, there are 15 almost two-dimensional free electron like bands in the lowest energy (-10 to -5 eV) region bearing mostly Cu $4s$ character and the bandwidth for $3d$ bands is $\sim$ 4 eV as in bulk Cu. Also the surface states are now almost degenerate at 0.6 eV below E_F at the Γ point are obtained. Therefore one can take the 15 layer slab as the system that is thick enough so that the two outer surfaces do not feel each other and this system forms the basis for our further investigation.

3.5   Slab consisting 15 Cu(111) planes

In order to study the electronic structure of Cu(111) slab, band structure and density of states of the slab containing 15 (111) planes are investigated within LMTO and Full potential methods.

The crystal structure is represented by a unit cell of length 76.16 a.u. including the spatial separation of 20.95 a.u. between two adjacent slabs within the full potential method. Position of the different atoms in Cu(111) planes in the structure file are fixed according to the symmetry of the structure and the length of the unit cell. In LMTO 15 Cu(111) planes and 6 layers of empty spheres are considered and the length of the unit cell is 82.824 a.u with 26.63 a.u. thick empty slab (a layered structure consisting of empty spheres only). The band structures calculated within Wien2k and LMTO are shown in Fig. 3.8.

Fig. 3.8 shows the surface state at Γ point is found 0.6 eV below Fermi energy in full potential. This is quite consistent with the experimental result since Shockley type surface states are detected by STM experiments [18] 0.4 $\pm$ 0.02 eV below the Fermi energy at Γ point. Recent Angle Resolved Photo Emission Spectroscopy (ARPES) experiment [38] observed surface state at 0.435 $\pm$ 0.001 eV below the Fermi energy at Γ point. However band structure calculated within the LMTO method the Shockley state is found at 0.13 eV below the Fermi energy at the Γ point. The rest of the band structure looks almost the same in both cases. Since the full potential method is very time consuming and we will have to increase our unit cell even further in the study of Co on Cu we try to correct the LMTO method so that we can use this in the future. Therefore we try to correct LMTO and bring the surface state at the same energy position as it is in the full potential band structure.

One can approach the problem in different ways. Our starting approach is to change the spatial separation between the surface Cu layer and the rest of the slab. The magnitudes of the coupling parameters between layers depend directly on their

spatial separation. Therefore by moving a layer towards or away from the slab one can effectively change the band structure. In Table 3.1 we show different separations (compare to the 4.83 a.u. separation of the layers corresponding to the bulk crystal structrure) between the layers and the energies of several features in the resulting band structures.

In the LMTO method a finite amount of overlaps between atomic spheres are considered. The program is designed to allow for less than 15 percent overlap between two atomic spheres while an atomic and an interstitial sphere are allowed to overlap by 20 percent. Therefore if the outermost plane is moved towards or away from the slab by a considerable amount, the radii of the atomic spheres in a plane should change. As the LMTO basis set depends on the size of these atomic spheres, their changes are expected to make considerable difference in the band structure. Within LMTO we find that an increase of 0.4 a.u. length between the two outer most Cu(111) planes and the rest of the slab changes both the radii of atoms in the outermost Cu(111) plane and the next empty sphere layer.

Our next approach is to change the nuclear charge of the outer most Cu(111) plane. Changing the nuclear charge means changing the potential which can simulate a shift in the band s. But we found that by changing the charge by only 0.1 the whole band structure of the outer most Cu plane is quite different as compared to the full potential band structure Fig. 3.9.

Next we try to adjust the band structure by applying an external potential to the top most Cu(111) layer. Applying a positive or negative potential means decreasing or increasing the electron density in that Cu layer. Table 3.2 shows the potentials applied on different orbitals of Cu plane and their effects in the band structure.

Our results in Table 3.1 and 3.2 justifies the reason behind our next step of applying a potential to the empty spheres to try to get a similar band structure compare to full potential. From fatband plots one can see that Cu $4p_z$ and the empty sphere $1s$ band couple strongly with each other. Therefore, by applying a potential to the $1s$ orbital of the empty sphere layer next to the Cu(111) plane one should be able to change the position of the surface state in the band structure without very much affecting the rest of the band structure. In table 3.3 the amount of potential applied to the empty sphere layer and the resulting changes noticed in the band structure are presented. In this case, by applying an attractive potential to the empty sphere plane we transfer some of the electron density of Cu(111) plane to this empty layer. Results show that, within LMTO method, -0.3 Ry potential applied to the s orbital of the empty layer gives a band structure almost similar compare to that of full potential together with the surface state at -0.55 eV.

Therefore we considered applying an external potential of -0.3 Ry to the s orbital of the nearest empty sphere plane in our later LMTO study of the electronic structure of the system. In conclusion of this section we have found that the surface electronic structure can be very well simulated with a slab thickness of 82.824 a.u. and a vacuum

Table 3.1: List of different distances between the outer most two Cu(111) planes (symmetry of the crystal structure gives that the separation between any two Cu(111) planes is $d = 4.83$ atomic unit (a.u.) along c axis) and changes in the corresponding band structures.

Length added to the separation between planes (in a.u.)	Position of the surface state at Γ point (in eV)	Change in radii of atoms and empty spheres	Changes noticed in the band structure
-0.5	-0.05	no change	Same as in the case of -0.4 a.u. distance addition
-0.4	-0.09	no change	$3d$ bands are different compare to Full potential
-0.3	-0.1	no change	Rest of the band structure is almost similar to that of Full potential
-0.2	-0.15	no change	$3d$ band near M point looks similar to that of Full potential
-0.1	-0.15	no change	$3d$ band near M point changes
0	-0.13	no change	Almost similar compare to Full potential band structure accept a $3d$ band at M point
0.1	-0.1	no change	No change in the rest of the band structure
0.2	-0.08	no change	$3d$ band near M point looks similar compare to Full potential
0.3	-0.02	no change	The band at M point crossing E_F starts to move away from E_F
0.4	0	radii change	The band at M point crossing E_F moves further away from E_F
0.5	-0.2	radii change	Band at M point crossing E_F is different compare to Full potential

Table 3.2: A table with different potentials applied on the last layer of Cu(111) plane and their outcome in the band structures.

Potential applied in Rydberg (Ry)	On orbital	Position of surface state at Γ point (in eV)	Changes noticed in the band structure
0.4	$4s$ and $4p$	-0.39	$4s$ bands change around K and M point
0.2	$4s$ and $4p$	-0.39	$4s$ bands change again around K and M point
0.1	$4s$ and $4p$	-0.25	$4s$ bands start to change around K and M point
0	none	-0.13	Almost similar compare to Full potential band structure accept a $3d$ band at M point
-0.1	$4s$ and $4p$	-0.12	$3d$ band changes near M point
-0.1	$4p$ only	-0.12	$3d$ band near M point changes
-0.1	$4s$ only	0	Band structure looks almost similar to that of Full potential

layer of 26.63 a.u. In order to get the surface state in LMTO and full potential at the same energy we can apply an external potential of -0.3 Ry to the empty spheres adjacent to the outermost Cu plane.

Table 3.3: A table with different potentials applied on the empty sphere plane next to the outer most Cu(111) plane in the slab and their outcome in the band structures.

Potential applied in Rydberg(Ry)	On orbital	Position of surface state at Γ point (in eV)	Main features of the band structure
0.4	$1s$ and $2p$	0.4	No change in the rest of the band structure
0	none	-0.13	A $3d$ band around M point in Full potential band structure is not present in LMTO
-0.4	$1s$ only	-0.7	A $3d$ band develops near M point which looks the same as in Full potential
-0.3	$1s$ only	-0.55	Almost similar band structure compare to Full potential
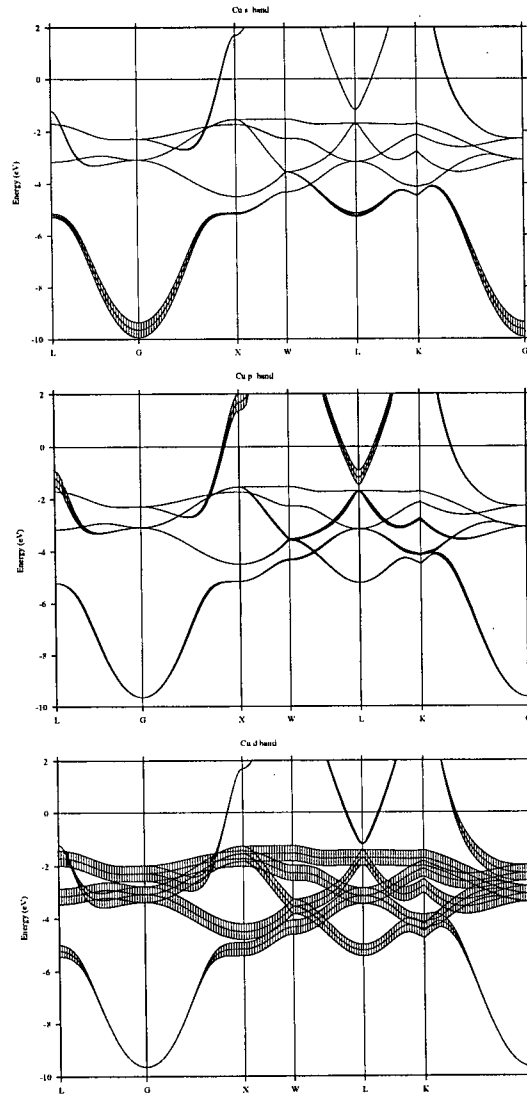
Figure 3.3: Fatband plots of $4s$, $4p$ and $3d$ bands for Cu bulk calculated within LMTO method. The first panel shows that $4s$ bands are at the lowest energy level. All the $3d$ bands are below E_F and bands crossing E_F have mainly $4p$ character.
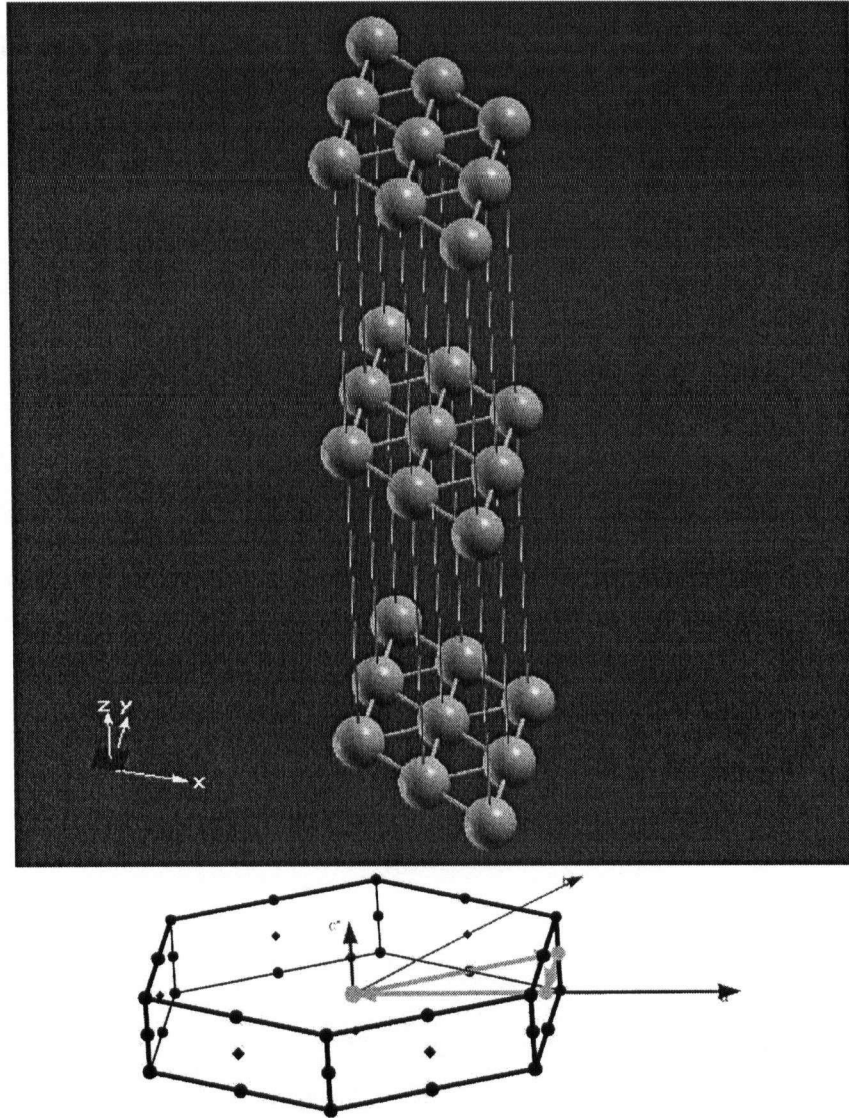
Figure 3.4: One layer of Cu(111) plane has triangular symmetry and these translation vectors ($\vec{a}_1 = 4.18322\hat{x} - 2.41518\hat{y}, \vec{a}_2 = 4.83037\hat{y}$ and $\vec{a}_3 = 20.94762\hat{z}$) map the crystal structure as shown in the above figure. Here all the lengths are in atomic units (a.u.). Hexagonal Brillouin zone for Cu(111) plane and the corresponding reciprocal lattice vectors ($\vec{b}_1 = 2\pi(0.23905\hat{x}), \vec{b}_2 = 2\pi(0.11953\hat{x} + 0.20702\hat{y})$ and $\vec{b}_3 = 2\pi(0.04774\hat{z})$).
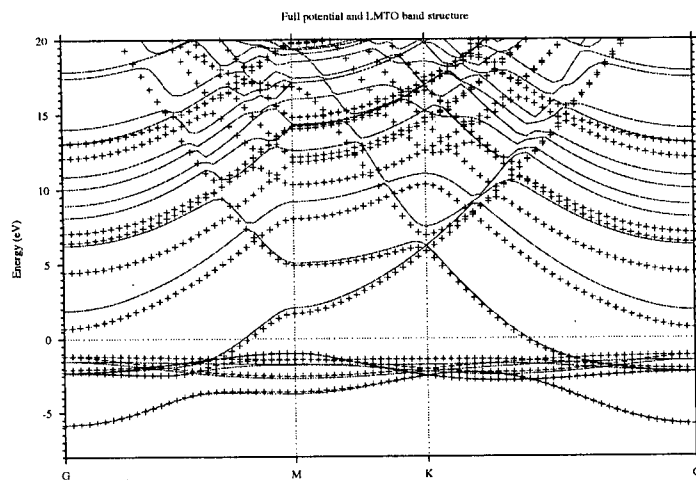
Figure 3.5: Band structure of a single layer of Cu(111) plane by LMTO and Full potential. Lines represents LMTO bands and points represents Full potential bands in the above figure.
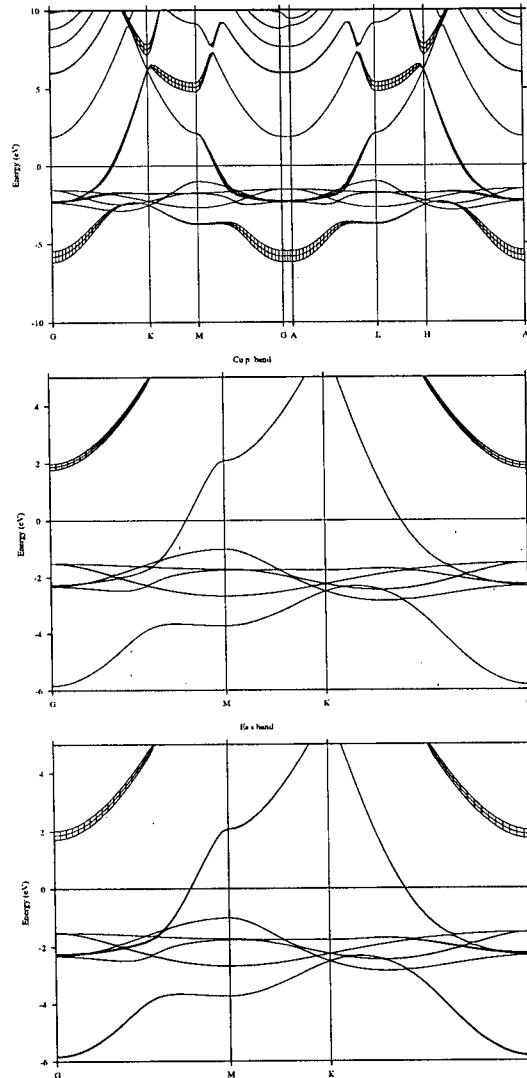
Figure 3.6: Fatband plot for Copper $4s$, $4p_z$ and empty sphere $1s$ bands. The width of all the bands have been decreased by sinificant amount and band crossing the Fermi energy has mostly $p_x + p_y$ orbital characters. Also one can see in the middle panel that $4p_z$ band is above the Fermi energy at Γ point.
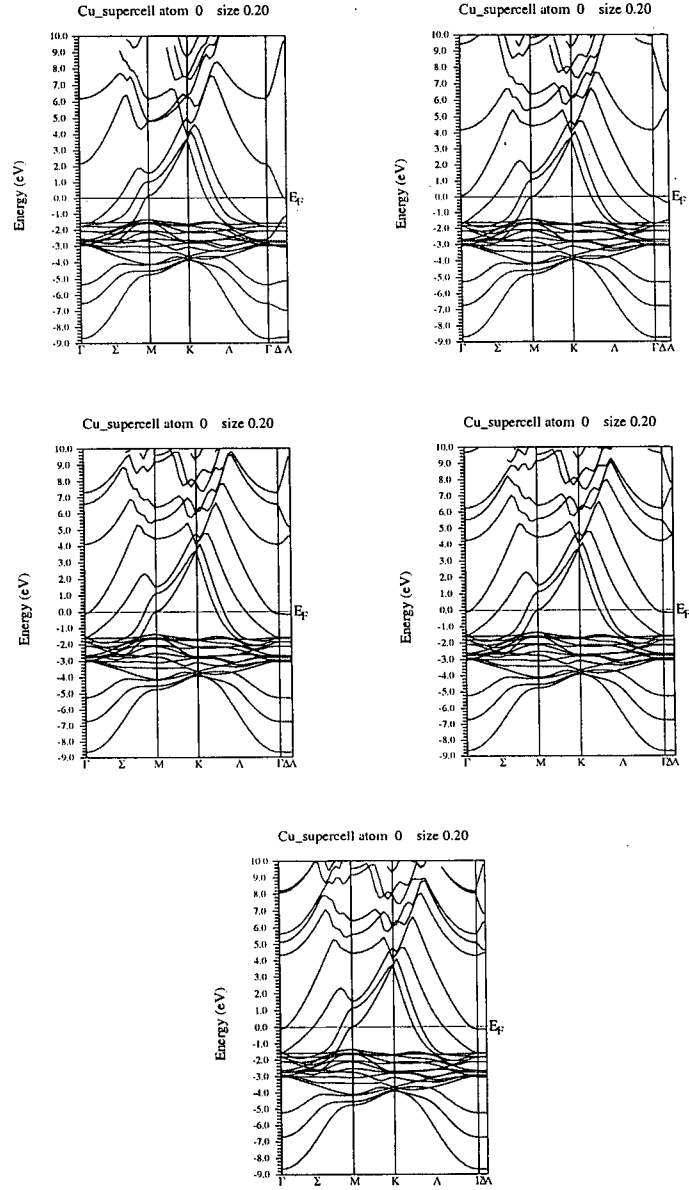
Figure 3.7: Self consistent full potential band structures of three Cu(111) planes with unit cell length 14.6 a.u., 19.2 a.u., 24 a.u., 28.8 a.u. and 33.6 a.u. along c axis. Band structure in the first panel shows dispersion in k_z along the high symmetry line of Γ to A. But with the increase of the length of the empty layer this k_z dispersion decreases. In the fifth panel we notice that for the empty layer of distance 20.95 a.u., the bands along the high symmetry line of Γ to A are almost dispersionless. Therefore with this length of the vacuum layer, slabs are successfully decoupled.
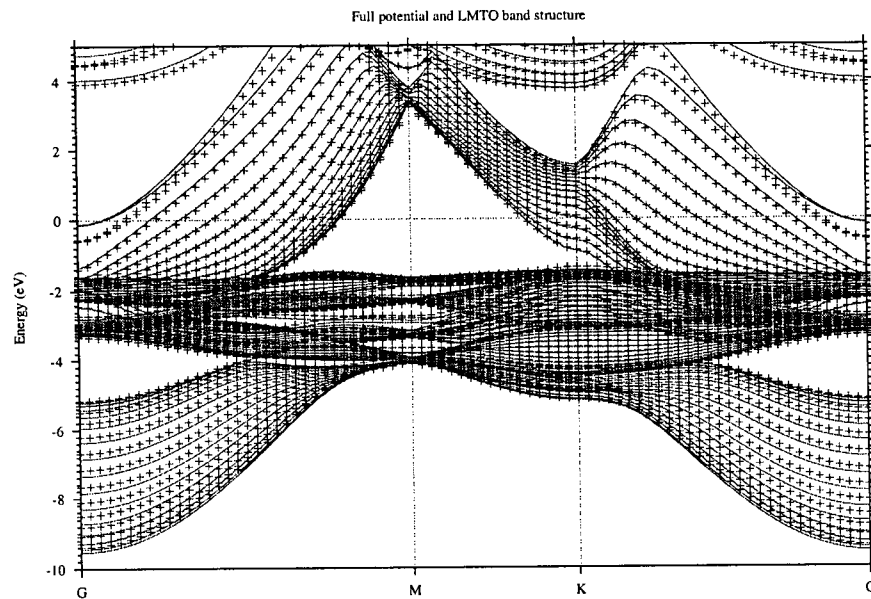
Figure 3.8: Band structures of 15 Cu(111) plane by Full potential and LMTO method where lines represents LMTO bands and points represents full potential bands. Both the band structures are almost similar accept the surface states at Γ point which are found to be at 0.6 eV and 0.13 eV below Fermi energy respectively in full potential and LMTO method.
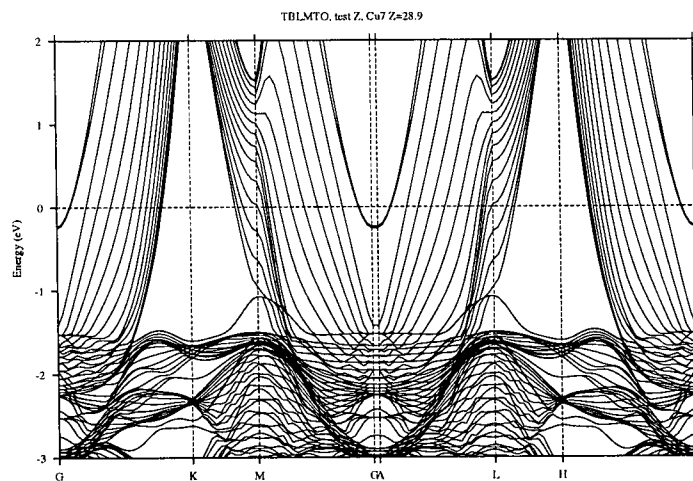
Figure 3.9: LMTO band structure of 15 Cu(111) planes with 28.9e charge on the outer most Cu plane.
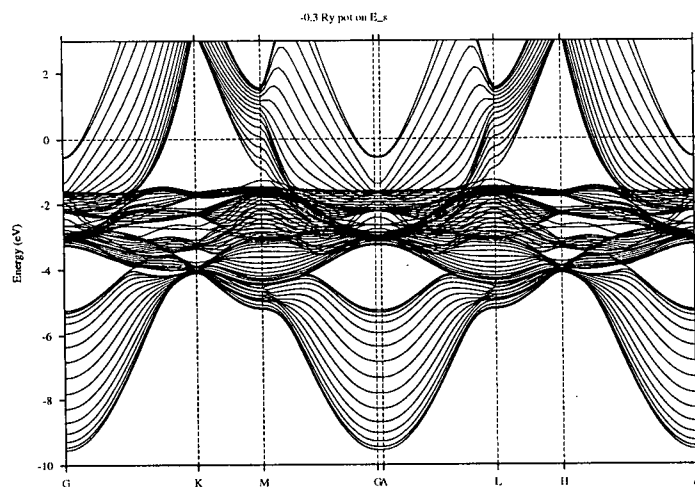
Figure 3.10: Band structure plot of 15 Cu(111) plane with -0.3 Ry potential applied on the 1s orbital of the nearest empty sphere plane.

Chapter 4

Electronic Structure of Co Adatoms on a Cu(111) Surface

When Co (a transition metal) is deposited on the non-magnetic metallic Cu(111) surface, the interaction between the electrons in the partially filled d shell of Co and the electrons of the metal results in interesting magnetic phenomena. To try to understand the magnetic properties of a Co impurity in this system we study the electronic structure of Co adatoms on a Cu(111) surface.

Let us start with a monolayer of Co deposited on a Cu(111) slab. As discussed in the previous chapter, a slab consisting of 15 Cu(111) planes has been chosen so that it is thick enough to decouple its two surfaces. At the same time it is possible to do calculations with our available CPU power and memory.

Fig. 4.1 shows the various spin polarized LDOS of one monolayer of Co on Cu(111) surface. We find for this system that Co is ferromagnetic. The total number of $3d$ electrons which is obtained by integrating the partial density of Co 3d states up to the Fermi energy is 7.23 in this case with the magnetic moment of 1.72 μ_B per Co. The majority of the states in the vicinity of Fermi energy are Co 'spin down' states with most of the 'spin up' states below it.

Even though the central layers of the Cu slab basically feels a cubic crystal field as in the bulk, the crystal field of the outermost Co layer is not cubic but trigonal. The point group symmetry of this trigonal crystal is D_{3d}. The e_g and t_{2g} orbitals in the cubic coordinate system are not the basis function of the irreducible representation of D_{3d}. One therefore chooses a new coordinate system to represent the basis functions of the irreducible representation of this group. In this new coordinate system the z axis is the threefold rotation axis chosen along the (111) direction, (z, x) is the mirror plane and y is the twofold rotation axis as shown in Fig. 11 of [40]. The five d orbitals in the new coordinate system are given by the following combination of the d orbitals in the cubic coordinate system (written in terms of x', y', z' axes)
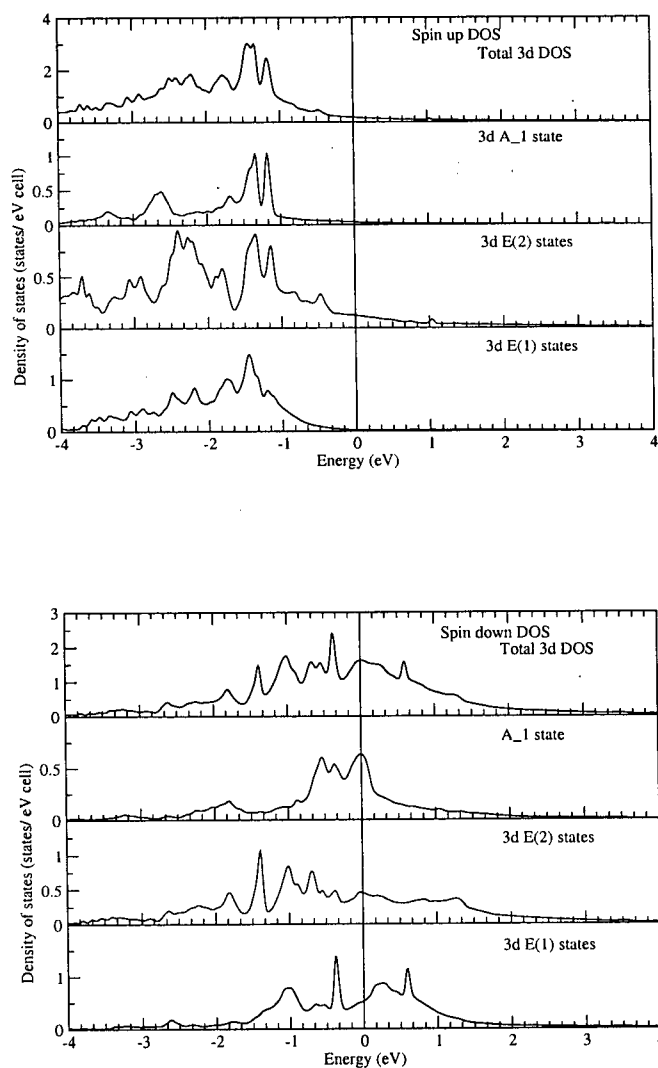
Figure 4.1: Density of states (DOS) plots for Co $3d$ electrons in the case of monolayer of Co on a Cu slab that contains 15 (111) planes. The upper panel shows DOS for the spin up electrons and the lower panel shows the spin up case. The zero energy is at Fermi energy. Most of the 'spin up' states are found below the Fermi energy while the 'spin down' states are centered around E_F.

$$|3z^2 - r^2\rangle = \frac{1}{\sqrt{3}}(|x'y'\rangle + |y'z'\rangle + |z'x'\rangle),$$

$$|yz\rangle = \frac{1}{\sqrt{6}}(2|(x')^2 - (y')^2\rangle - |y'z'\rangle + |z'x'\rangle),$$

$$|zx\rangle = \sqrt{\frac{2}{3}}|3(z')^2 - r^2\rangle - \frac{\sqrt{2}}{6}(2|x'y'\rangle - |y'z'\rangle - |z'x'\rangle),$$

$$|xy\rangle = \frac{1}{\sqrt{3}}(-|(x')^2 - (y')^2\rangle - |y'z'\rangle + |z'x'\rangle),$$

$$|x^2 - y^2\rangle = \frac{1}{\sqrt{3}}|3(z')^2 - r^2\rangle - \frac{1}{3}(2|x'y'\rangle - |y'z'\rangle - |z'x'\rangle). \tag{4.1}$$

These five d orbitals are categorized into three groups according to the irreducible representations of D_{3d}. $|3z^2 - r^2\rangle$ is called A_1, $|yz\rangle$ and $|zx\rangle$ are called $E(1)$ and $|x^2 - y^2\rangle$ and $|xy\rangle$ are called $E(2)$.

Fatband plots show that in this crystal field, the degeneracy of the Co $3d$ orbital is partly lifted and we get a non-degenerate A_1 band and doubly degenerate bands for $E(1)$ and $E(2)$.

Our goal is to study the electronic properties of a Co adatom on Cu(111). To do this and still make use of the powerful band structure software we need to still have a periodic structure of Co adatoms in the x, y plane. These atoms though should be far enough apart that interactions between them is negligible. We start with a Co adtom layer in a 2 × 2 supercell in x and y directions. Together with the 15 Cu(111) layers in each slab and two Co atom, there are altogether 95 atoms in a unit cell. This is already a very large calculation which slows down the computational speed by a considerable amount. Apparently the problem of spending memory and CPU time can be avoided by trying to preserve symmetry of the system as much as possible. Ideally one would like to have one Co atom in a supercell to study its electronic structure on the Cu surface. But Co on both sides of the slab is the most symmetric case for the system under consideration. At the same time, the number of Cu(111) planes in the slab is reduced from 15 to 11 for similar reasoning. The crystal structure is simulated by making a slab of 13 Cu(111) planes using $P - 3m1$ symmetry of the Cu(111) slab and then replacing the outermost layers of Cu(111) planes by a 2 × 2 superstructure of Co atoms with less number of Co atoms per plane compare to Cu. The calculation is done for the two cases a Co layer only on one side giving an antisymmetric situation and the more symmetrical case of a Co layer on both sides. The results are presented in Fig. 4.2.

Fig. 4.2 shows no significant difference in the projected DOS plots of the symmetric and asymmetric combinations. Since the self consistent density functional calculation for asymmetric slab takes much more computer time, we choose to work
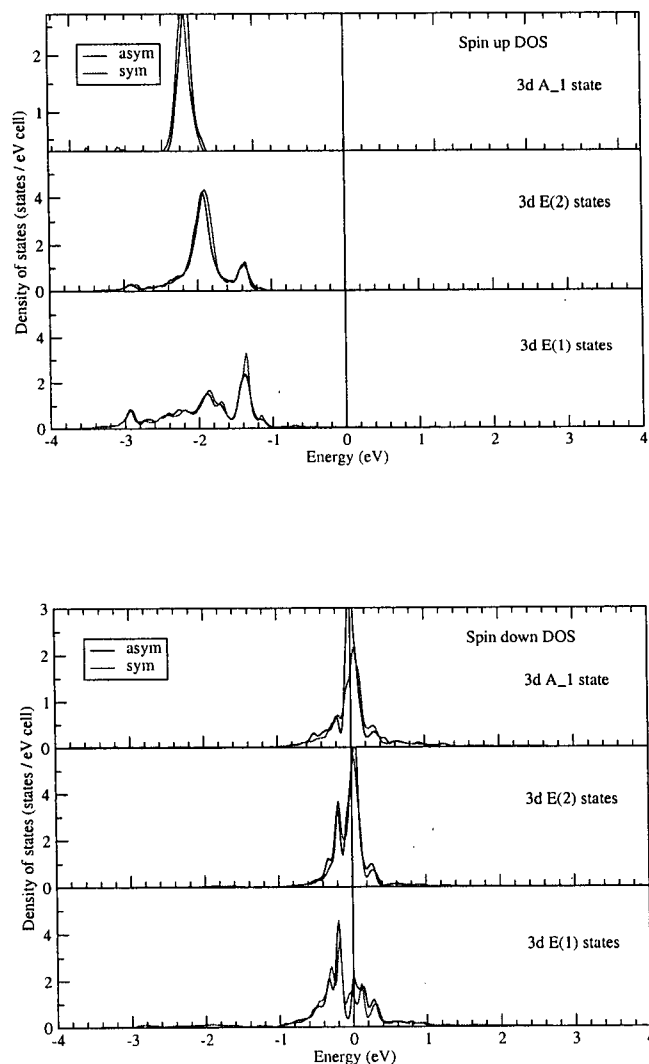
Figure 4.2: Density of state (DOS) plots of Co $3d$ 'spin up' (the upper panel) and 'spin down' (the lower panel) states for asymmetric (one Co atom on one side of Cu slab) and symmetric (two Co atoms, one on each side of the outer most Cu planes) slabs calculated within full potential method. A 2×2 supercell is considered in these calculations. The zero of energy is at Fermi energy.

with a symmetric slab with Co impurity on Cu(111) surface.

From Fig. 4.2 we see that the overall width of the Co A_1 states (in the local coordinate system) is about 0.5 eV together with some dips and peaks in the DOS. The width of the Co d states can result from two main mechanisms. The coupling of the Co-d states with a Cu sp bands, resulting in a kind of virtual bound state with a width given by $2\pi|V_{\mathbf{k}d}|^2$ times DOS as described in chapter 1 for the Anderson model. Secondly the d states can attain a dispersional width because we have placed them in a lattice. The coupling between Co-d orbitals on neighboring Co sites can lead to a dispersional band width which could be important because the supercell under consideration is relatively small. But this is quite unlikely because d orbitals are quite compact and the coupling parameter between two d orbital is inversely proportional to the fifth power of the spatial separation between the atoms [39]. Of course one should also take into account the indirect hoping via Cu states but also these are probably quite small. Following Harrison [39] the hopping parameters between sp-d orbital and d-d are given by

$$V_{ldm} = \eta_{ldm}\frac{\hbar^2 r_d^{3/2}}{md^{7/2}},\ V_{ddm} = \eta_{ddm}\frac{\hbar^2 r_d^3}{md^5} \tag{4.2}$$

where l is any of the s and p orbital, m stands for σ or π bonding, η's are dimensionless universal constants also mentioned in [39] for different cases of l and m and d is the distance between atoms. The most important point to notice here is that these coupling parameters are inversely proportional to the spatial separation between atoms. It decreases rapidly with the increase of d in the above expression.

To make sure the origin of the widths for Co d states, a larger (3×3) supercell has been investigated and the resulting DOS calculated within self consistent full potential method are compared to the 2x2 super cell in Fig.(4.3). The calculation with a 2×2 supercell shows that the total number of $3d$ electrons is 7.24 with the magnetic moment of $1.97\mu_B$. In a 3×3 supercell the total number of $3d$ electrons is 7.24 with the magnetic moment of $2.00\mu_B$. These numbers together with the DOS plots indicate that there is no significant difference between 2×2 and 3×3 supercell cases. One can therefore say that coupling between Co-d orbitals of two different Co atoms is not very strong even in the case of 2×2 supercell. The width in the DOS of Co d bands is coming from the coupling between Co d and the Cu sp surface and bulk states. Hence our final choice for studying the electronic structure of Co impurity on Cu(111) surface is the slab having 2×2 supercell geometry with 15 Cu(111) planes along z axis and two Co atom per supercell (one on each side of the slab).

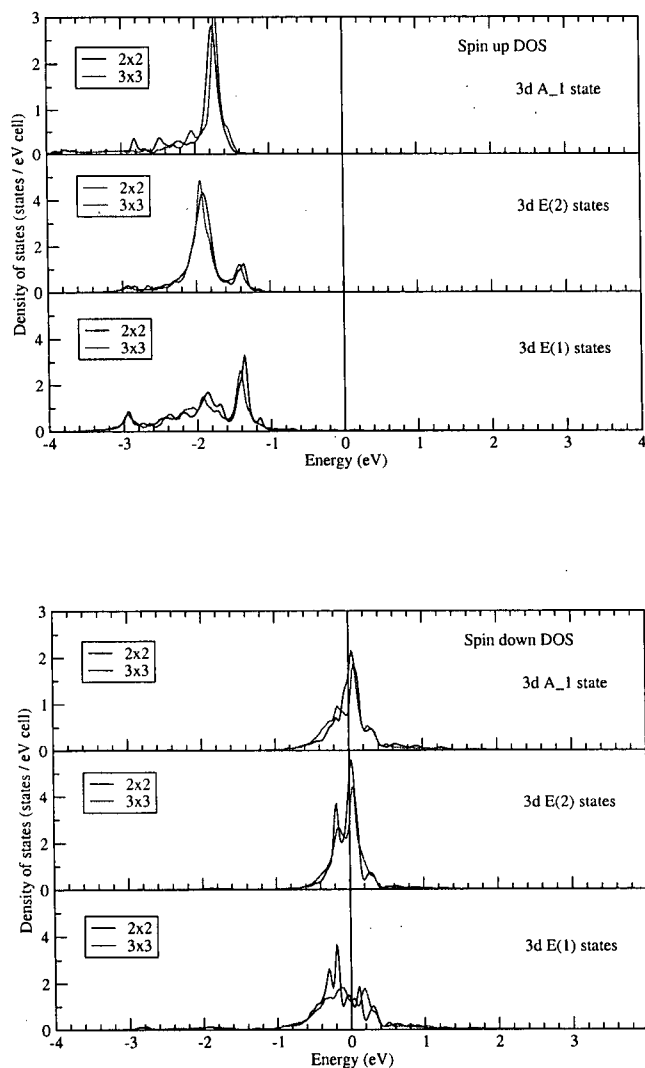Figure 4.3: Density of state (DOS) plots of Co $3d$ spin up and down states for 2×2 and 3×3 supercell structures (with two Co atoms per unit supercell of 11 layer Cu slab, calculated within full potential method) are shown in the upper and lower panel, respectively. The zero of energy is at Fermi energy. There is no significant difference in the DOS for both spin up and down states.

4.1 Optimal Co-Cu distance

So far we have been using the distance between Co adatom with the Cu surface which is same as the distance between two Cu(111) planes in the slab. The width of Co d states is coming mainly from the coupling of these states with Cu sp surface and bulk states. Coupling parameters change with the distance between atoms under consideration. Therefore a change in the vertical distance between Co adsorbate and Cu surface can result in significant change in the Co d density of states. It can also change the widths of different DOS together with their shapes. The *ab initio* density functional calculations provide the total ground state energy which can be used to find the equilibrium vertical position of the Co atom on the Cu(111) surface.

Density functional method is based on the Born-Oppenheimer approximation that says, due to their heavy masses nuclei moves much slower than the electrons, therefore one can consider the electrons as moving in a field of fixed nuclei with zero nuclear kinetic energy and a constant nuclear potential energy. In this situation one can treat each configuration in the adiabatic limit to find the configuration with lowest total energy. Therefore one looks for the lowest total energy configuration for a slab that contains 15 Cu(111) planes together with two Co atoms in a 2 × 2 supercell.

Full potential calculation is the most accurate method for calculating the total energy of the system. Although LMTO is very similar to full potential, once Co is moved from the equilibrium position due to atomic sphere approximation, the total energy becomes completely different compare to that of full potential.

Fig. 4.4 is a plot of different total energies as a function of the change in spatial separation between Co adatom and Cu(111) surface. We find within full potential method that a spatial separation of 4.79 a.u. between the Co adatom and Cu surface yields the lowest total energy configuration for our system. The difference between the total energy of the configuration with equilibrium distance between Co adatom and Cu surface and the configuration with lowest total energy is found to be ~ 1 eV per unit cell and so is very significant. Since there are 2 Co atoms per unit cell, the change in energy associated with each Co atom is 0.5 eV. Fig. 4.5 shows the DOS of spin down Co d A_1 states for different distances between the Co adatom and Cu surface and we chose the second case of lowest total energy configuration for further investigation.

From LMTO calculations of this system with the optimal distance between Co adatom and Cu surface we find that there are 7.56 electrons in the $3d$ orbitals with the magnetic moment of 1.70 μ_B per Co. Full potential calculation gives that there are 6.47 electrons in the $3d$ orbitals with the magnetic moment of 1.71 μ_B per Co. One notice that in the full potential calculation of the Co/Cu(111) optimal distance, due to the proper treatment of the atomic potential inside and outside of the muffin-tin sphere, the radius of the muffin-tin sphere decreases. Hence the amount of d electron present inside the atomic sphere (we integrate the electron density inside the sphere)
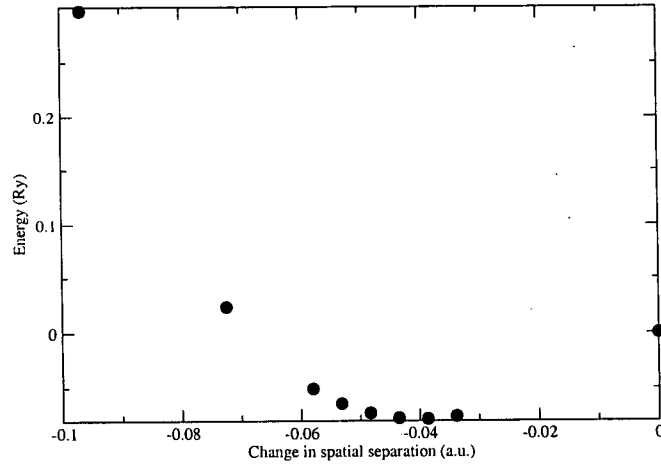
Figure 4.4: Total energy as a function of the distance between Co adatom and Cu(111) surface. The zero of energy corresponds to the total energy of a configuration when the distance between the Co adatom and Cu surface is 4.83 a.u. We notice that, total energy has a minimum for the system when the distance between Co adatom and Cu(111) surface is 4.79 a.u.

is smaller compare to that of the previous full potential calculation.

Fig. 4.6 shows DOS plots for bands carrying different orbital characters calculated within Wien2k full potential method. We find that the DOS for spin up electrons are centered below the Fermi energy and that for spin down electrons are mostly centered at the Fermi energy. Therefore we can comment that for spin up electrons all five $3d$ orbitals are almost filled together with some unfilled orbitals for spin down electrons.

Although the shapes of the density of states calculated within these two methods differ, the band widths look almost comparable in case of $4s$, $4p$ and $3d$ bands. Comparison of DOS plots from LMTO and full potential method shows that the width of the Co d A_1 is 0.5 eV in both cases.

One cannot definitely say that in the experiment one directly observes the DOS found from these single particle pictures. The dI/dV spectra is interpreted to measure the local density of states times the tunneling matrix element squared. Therefore presence of an eigenstate that is a linear combination of atomic states with coefficients (that are strongly energy dependent) makes the tunneling matrix element (which also becomes energy dependent) much more complicated. In such a situation it is
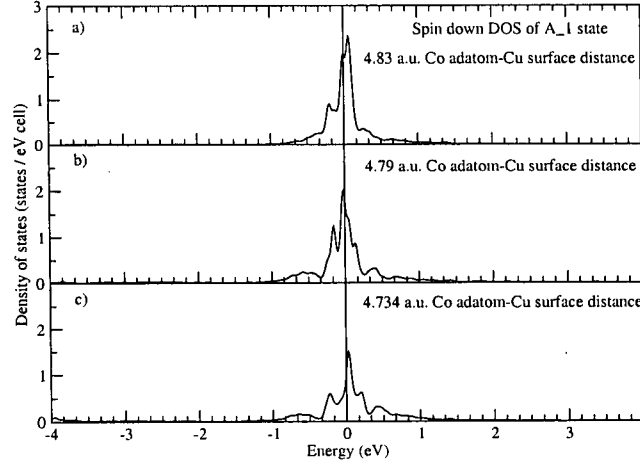
Figure 4.5: Partial DOS of A_1 state in the case of three distances between Co adatom and Cu(111) surface. DOS for optimal distance is shown in the middle panel. The zero of energy is at Fermi energy.

important to know which atomic states are mostly responsible for tunneling and also the corresponding tunneling strengths. Here the radial parts of the orbital wave functions are equally important together with the angular symmetry.

An orbital character study of the band structure is carried on in this situation. Fig. 4.7 is a three dimensional plot of the LMTO band structure and the projection of the eigenfunction onto Co d A_1 state. That is we plot the wave vector k and energy eigenvalues in the x, y plane and $M_{\mathbf{k}}^n = \sum_{i=1}^2 \langle \psi_{\mathbf{k}}^n | (3z^2 - r^2)_i \rangle \langle (3z^2 - r^2)_i | \psi_{\mathbf{k}}^n \rangle$ along z axis. It is like fatbands but without the scaling factor multiplied that is used in plotting them. This 3D plot shows that near the Fermi energy at the Γ point Co d A_1 state strongly mixes with Cu sp surface and bulk states present in the vicinity of Co atom. At K point the height of this band is almost 0.8 meaning that at this point, the eigenfunction has mostly Co d A_1 character that does not mix with Cu states.

At this point Co d electron spin density in real space is studied. The density distribution for spin up and down states can be written as $\rho_{\uparrow/\downarrow}(\mathbf{r}) = \sum_{i=1}^N n_{i\uparrow/\downarrow} |\phi_{i\uparrow/\downarrow}(\mathbf{r})|^2$. Here n_i is the occupation number and ϕ_i is the eigenfunction of Kohn-Sham Eq. Electron spin density is defined as $\rho_s = \rho_\uparrow - \rho_\downarrow$ where $\rho_\uparrow$ and $\rho_\downarrow$ represents density of spin up and spin down electrons, respectively.

The electron spin density of half of the slab is shown in Fig. 4.8 where we consider
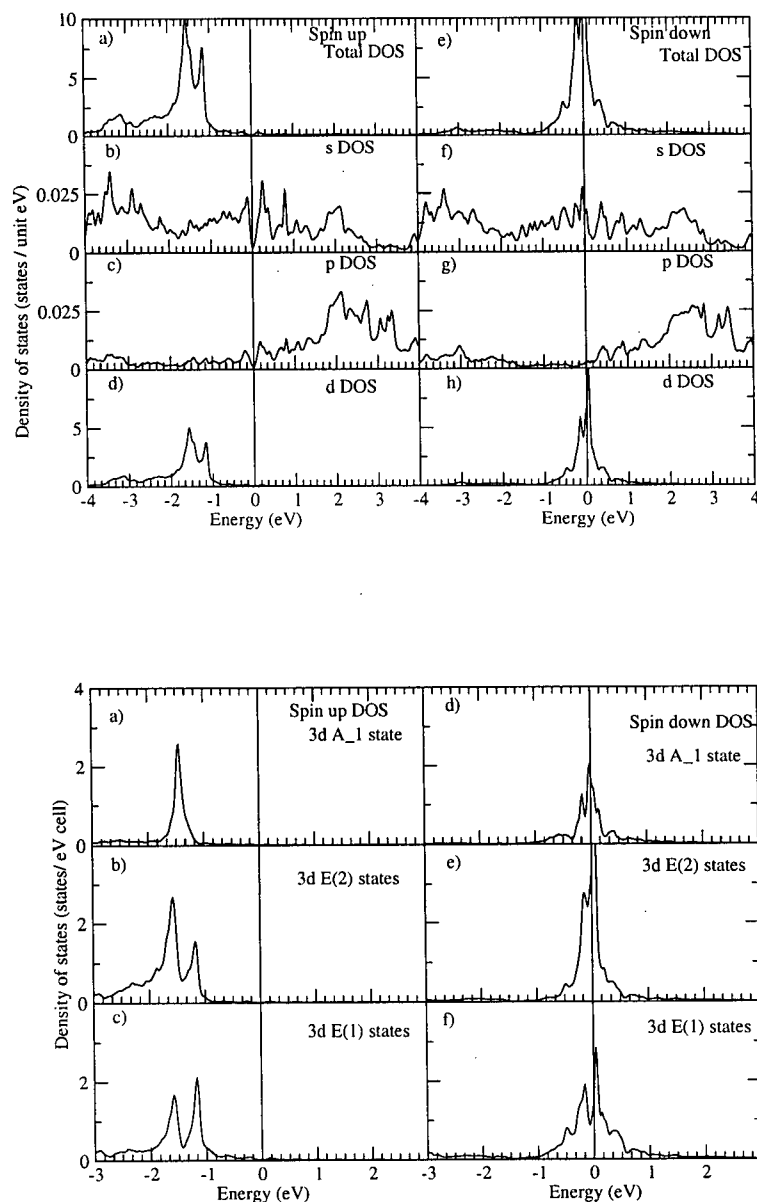
Figure 4.6: The upper panel shows total and partial density of states for Co $4s$, $4p$ and $3d$ spin up and spin down electrons in the case of optimal Co adatom and Cu surface distance calculated within full potential method. The lower panel shows partial density of states (PDOS) of different $3d$ states. One can see from the lower panel PDOS that all the spin up states are filled (centered below E_F) and spin down states are partially filled (PDOS centered at the E_F). The zero of energy is at Fermi energy.
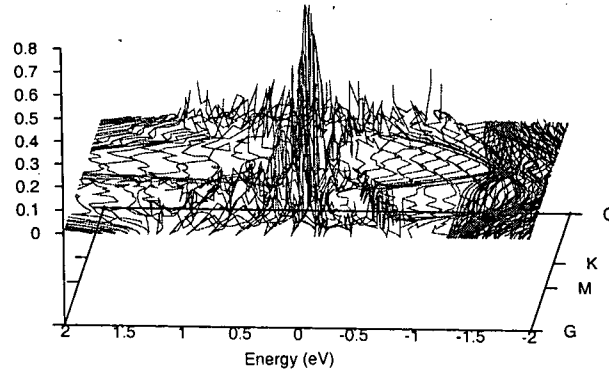
Figure 4.7: LMTO band structure of Co/Cu (111) calculated for optimized Co-Cu distance. Co d $3z^2 - r^2$ coefficient squared is plotted in the z axis.

two 2×2 supercells in both x and y directions. The isosurfaces represented by red and blue show the surfaces of constant spin density of 0.005 and -0.005 electrons per unit volume, respectively. Since Co has rather large magnetic moment, the Cu states are spin polarized too which leads to the spin density extended throughout the whole Cu slab. As described in chapter 3, one needs four Cu atoms per plane to map a 2×2 supercell structure. These four Cu atoms can be categorized into two groups with respect to the position of the Co atom. First type of Cu atoms have multiplicity 3 that belongs to those triangles which has Co atom sitting on the threefold rotation axis on the plane above the triangle. Second type of Cu has multiplicity 1 and sits at the center of the 2×2 supercell in the x, y plane. The magnetic moments of these different Cu atoms induced by Co are listed in Table 4.1. The values of the magnetic moments together with Fig. 4.8 shows clearly that magnetism propagates throughout the whole slab.

However one needs to look at the spin density distribution at this point since these numbers don't tell us how and where exactly the spin states are present in the real space. From Fig. 4.8 we notice that the spin density is asymmetric in shape and also there is a large negative spin density blanket (the large blue shapes present between the Co adatoms and the first Cu layer) between Co and first Cu layer. Also the coupling between Co d states and Cu conduction electron states is anti-ferromagnetic

Table 4.1: List of the magnetic moments on different Cu atoms in the Cu layers of half of the slab.

Cu plane number	Magnetic moment on Cu with multiplicity 3 (μ_B per Cu)	Magnetic moment on Cu with multiplicity 1 (μ_B per Cu)
First	-0.0071	0.0114
Second	-0.0136	-0.0126
Third	-0.0041	-0.0075
Fourth	0.0117	0.0082
Fifth	0.0007	-0.0019
Sixth	-0.0052	-0.0069
Seventh	-0.0002	-0.0028
Eighth (middle most)	0.0065	0.0044

which results in a small magnetic moment on Cu in the first layer. From Fig. 4.8 one can immediately see that the large spin down density compensates almost all of the spin up density in the muffin tin sphere of Cu in the first layer. The density distribution is so anisotropic that we get a small negative magnetic moment for Cu atoms with multiplicity 3 (which is the integral of the spin density over the muffin tin sphere) and a small positive number for that of the Cu atoms with multiplicity 1 in the first layer.
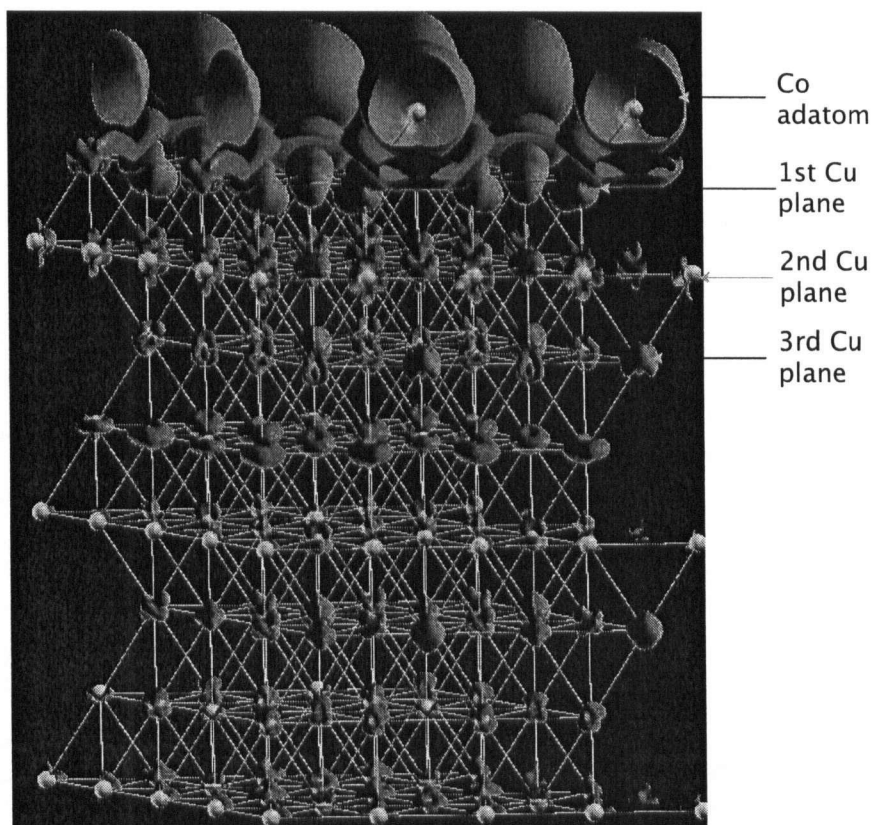
Figure 4.8: This is a plot of electron spin density of half of the slab with 2×2 supercell structure. The number of unit cells is doubled in x and y directions. 0.005 and -0.005 spin density isosurfaces are represented by red and blue colors, respectively (calculated within LMTO method). Large red spheres at the top most layer represents Co atoms and the remaining seven layers are Cu(111) planes. As one can see magnetism propagates through the whole slab since we observe some (small or large) amount of both positive and negative spin density present in all layers of Cu.
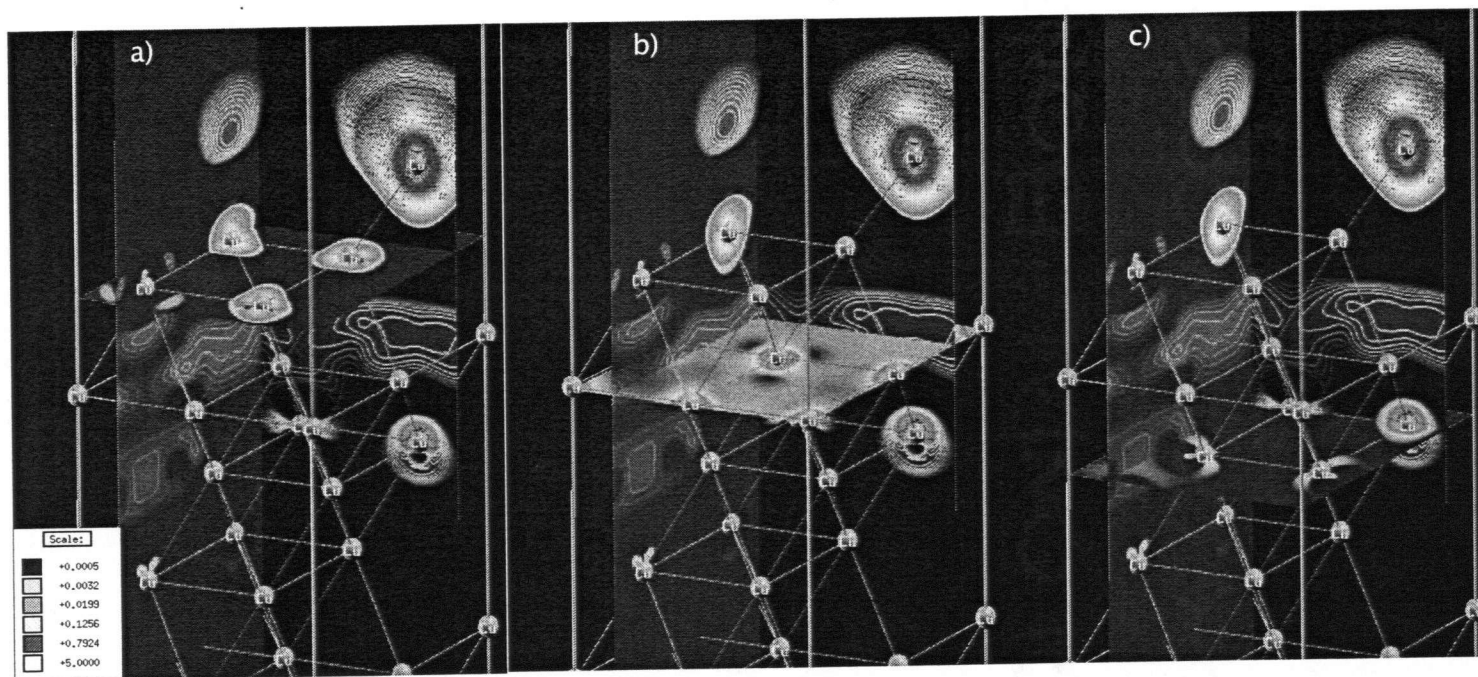
Figure 4.9: Three panels with cuts through three different Cu layers are shown here. Isolines show only positive spin density and this is only one unit cell. In the first panel the horizontal cut shows the Cu spin density in the first Cu plane. Similarly in the second and third panels cuts show the spin densities in the second and third Cu planes, respectively. One can see that in the second plane the spin density is quite spread all over the plane while they are relatively concentrated around Cu atom in other planes. The second Cu layer is therefore different from any other Cu layers.

In Fig. 4.9 the isolines show only positive spin density. We notice that the second layer of Cu has the highest magnetic moment per Cu among all other layers although the its magnitude is quite comparable in other layers. As one can see from Fig. 4.9, the spin density is spread over the whole second Cu plane but it is highly concentrated around Cu sites in all other layers. Therefore we conclude that it is important to consider the spin density distribution since it is very anisotropic and gives rise to almost comparable magnetic moments through the whole Cu slab.

Fig. 4.10 shows the Co electron spin down density for all Co *spd* states integrated in the energy window -0.2 to +0.2 Ry around the Fermi energy. As expected, the spin density has highest value at the center of the Co atom and the value decreases as one moves away from Co. This picture tells us that Co *spd* states mix with the first Cu layer states pretty strongly since we see some Co spin density in that layer. Cu states are not present in this picture because the occupation number for all those states are set to zero. The isolines in this picture correspond to different spin densities as indicated in the thermometer.

The above investigation shows that a 2×2 symmetric supercell consisting of 15 Cu(111) planes with 2 Co atoms one on each side of the slab is sufficient for studying the electronic properties of Co adatoms on a Cu(111) surface. We find that Co $3d$ states are split into non-degenerate A_1 and two doubly degenerate $E(1)$ and $E(2)$ states by the surface potential of trigonal symmetry. Note that the Co adatom is not at a inversion center. Therefore Co p and d states can mix. In addition, we find that the width of the Co d states mainly arise from the coupling to Cu sp surface and bulk states. The calculated number of Co d electrons is 7.56 with the magnetic moment of 1.7 μ_B per Co which is consistent with a d^8 configuration of Co in the high spin state. The spin density calculated within the LMTO scheme shows a much longer range as compared to the part of the charge density associated with Co states. It is interesting to note that the induced magnetic moment in the second Cu layer is even bigger than the magnetic moment in the first layer.

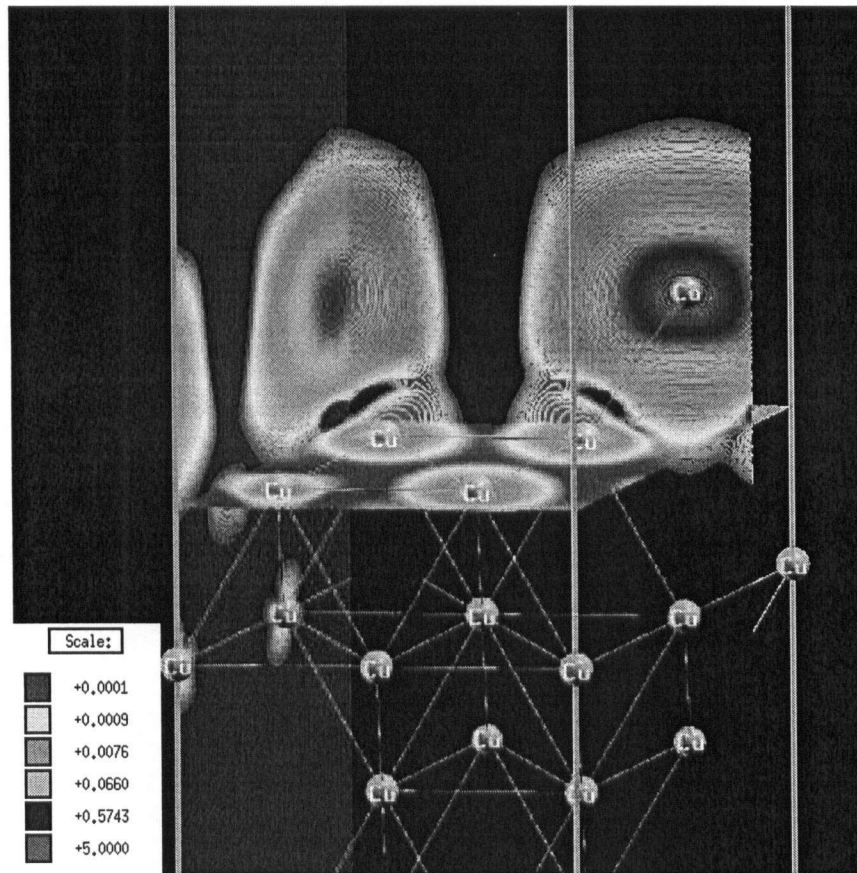Figure 4.10: The above picture shows the Co spin down density for all Co states in the energy window of -0.2 to +0.2 Ry around Fermi energy (calculated within LMTO method). The isolines corresponding to different spin densities are shown in this picture. There is only one Co per unit cell. The part of density on the left of Co is coming from the neighboring cell. The horizontal cut shows Co density in the top Cu layer.

Chapter 5

Outlook

5.1 Tight Binding Hamiltonian for 1 layer of Cu(111) plane

With the knowledge of a basis set and relative hopping parameters one can write down the Hamiltonian matrix for a specific system in the tight binding method. Therefore solving the Hamiltonian one gets the eigenstates and eigenvalues hence the band structure.

Our initial interest was to write a model Hamiltonian with approximate numerical values for important hopping parameters between orbitals of the magnetic system of Co adatom on Cu(111) surface. Therefore we started with a single Cu(111) plane. Density functional calculation for Cu(111) slab shows that sp type states are present near the Fermi energy. Hence only $4s$ and $4p$ orbitals are chosen to represent each atoms in plane and the nearest neighbor hopping is considered between atomic orbitals. If the nearest neighbor hopping is mainly important for the system under consideration, almost similar band structure is expected from tight binding model compare to that of LMTO. For a single Cu(111) plane, band structure calculated in tight binding method seemed to match pretty well with the band structure that we get from LMTO.

Following is a description of the model Hamiltonian that we have for a single Cu(111) plane. As mentioned, $4s$ and $4p$ orbitals are chosen to represent each atoms in the plane together with the nearest neighbor hopping only. Even though this is not a complete description of the system, it can help us getting approximate numerical values for hopping parameters. A mathematical package (MAPLE) is used to get the eigenvalues and the eigenvectors. The eigenvalues are plotted as a function of the wave vector to get the associated band structure.

The basis set is written as $\{|4s\rangle \equiv |1\rangle, |4p_x\rangle \equiv |2\rangle, |4p_y\rangle \equiv |3\rangle, |4p_z\rangle \equiv |4\rangle\}$. The 4×4 Hamiltonian matrix is written in terms of this basis set is given by:

$$H = \begin{pmatrix} H_{11} & H_{12} & H_{13} & H_{14} \\ H_{21} & H_{22} & H_{23} & H_{24} \\ H_{31} & H_{32} & H_{33} & H_{34} \\ H_{41} & H_{42} & H_{43} & H_{44} \end{pmatrix}$$

where H_{ij} stands for $\langle i|H|j\rangle$. The nearest neighbor hopping parameter between

different orbitals are represented by $t_{ss\sigma} = \sigma$ hopping between $s - s$ orbitals, $t_{sp\sigma} = \sigma$ hopping between $s - p$ orbitals, $t_{pp\sigma} = \sigma$ hopping between $p - p$ orbitals and $t_{pp\pi} = \pi$ hopping between $p - p$ orbitals. In the (111) plane one Cu atom has six nearest neighbors. The coordinates of an atom (O) and its six nearest neighbors $(A_1, A_2, A_3, A_4, A_5$ and $A_6)$ are (0,0,0) and (a,0,0), (a/2,$\sqrt{3}a/2$,0), (-a/2,$\sqrt{3}a/2$,0),(-a,0,0),(-a/2,-$\sqrt{3}a/2$,0) and (a/2,-$\sqrt{3}a/2$,0), respectively.

Elements of this symmetric Hamiltonian matrix are the following

$$H_{11} = 2t_{ss\sigma}\{\cos(\mathbf{k} \cdot \mathbf{r}_1) + \cos(\mathbf{k} \cdot \mathbf{r}_2) + \cos(\mathbf{k} \cdot \mathbf{r}_3)\}$$

$$H_{12} = 1.732it_{sp\sigma}\{\sin(\mathbf{k} \cdot \mathbf{r}_2) + \sin(\mathbf{k} \cdot \mathbf{r}_3)\}$$

$$H_{13} = it_{sp\sigma}\{2\sin(\mathbf{k} \cdot \mathbf{r}_1) + \sin(\mathbf{k} \cdot \mathbf{r}_2) - \sin(\mathbf{k} \cdot \mathbf{r}_3)\}$$

$$H_{14} = 0$$

$$H_{22} = E_p + 2t_{pp\pi}\cos(\mathbf{k} \cdot \mathbf{r}_1) + (1.5t_{pp\sigma} + 0.5t_{pp\pi})\{\cos(\mathbf{k} \cdot \mathbf{r}_2) + \cos(\mathbf{k} \cdot \mathbf{r}_3)\}$$

$$H_{23} = 0.866(t_{pp\sigma} - t_{pp\pi})\{\cos(\mathbf{k} \cdot \mathbf{r}_2) - \cos(\mathbf{k} \cdot \mathbf{r}_3)\}$$

$$H_{24} = 0$$

$$H_{33} = E_p + 2t_{pp\sigma}\cos(\mathbf{k} \cdot \mathbf{r}_1) + (0.5t_{pp\sigma} + 1.5t_{pp\pi})\{\cos(\mathbf{k} \cdot \mathbf{r}_2) + \cos(\mathbf{k} \cdot \mathbf{r}_3)\}$$

$$H_{34} = 0$$

$$H_{44} = E_{p_z} + 2t_{pp\pi}\{\cos(\mathbf{k} \cdot \mathbf{r}_1) + \cos(\mathbf{k} \cdot \mathbf{r}_2) + \cos(\mathbf{k} \cdot \mathbf{r}_3)\}$$

where k is the reciprocal lattice vector in k space. Here $\mathbf{r}_1 = A_1$ and $-\mathbf{r}_1 = A_4$ and so on. Also in this symmetric matrix $H_{21} = H_{12}^*$, $H_{31} = H_{13}^*$... E_p and E_{p_z} are the crystal field splitting for (p_x, p_y) and p_z states. The resulting band structure is then compared with that of LMTO. Fitting of these two band structures give us relatively acceptable numerical values for the hopping parameters from tight binding method.

Next we tried adding more Cu(111) planes according to the symmetry of the crystal. But as more Cu(111) layers were added to the single Cu(111) plane, we found it quite difficult to fit the band structure from our model hamiltonian and that from the LMTO. Therefore we conclude that the next-nearest, next-next-nearest neighbor and so on hopping should be considered for the proper treatment of the system.

5.2 Summary and outlook

We have presented a rather detailed *ab initio* study of the electronic structure of Co adatoms on Cu(111) surface. A careful look at the band structure and orbital characters of Cu bulk showed that $4p$ bands are dominantly present near Fermi energy. The band structure of a single Cu(111) plane shows that the band widths corresponding to bands with different orbital charaters are reduced by considerable amount. With the increase of number of layers in the slab this band width is regained. Finally we

find that a slab thickness of 82.824 a.u. and a vacuum layer of 26.63 a.u. is our choice for studying the surface electronic properties of Cu(111) slab. An external potential of -0.3 Ry applied to the nearest empty sphere layer within LMTO method gives surface state at the same energy (-0.55 eV) compare to Full potential.

In chapter 4 the electronic structure of Co adatoms on Cu(111) surface is investigated. Self consistent density functional calculation of Co monolayer on Cu(111) surface shows that Co is magnetic in this system. We find that a 2×2 supercell in x, y direction is sufficient for studying electronic structure of Co impurity. Trigonal crystal field at the surface of this simulated Cu(111) slab lifted the degeneracy on the Co d states and non-degenerate A_1 state and doubly degenerate $E(1)$ and $E(2)$ states are observed. The lowest total energy of the system is calculated when the distance between Co adatom and Cu surface is 4.79 a.u. The change in energy (difference between total energies of the configurations with 4.83 a.u. and 4.79 a.u. distances between Co adatom and Cu surface) associated with each Co atom is found to be 0.5 eV.

Partial density of states (PDOS) plots for different Co d states show that all the spin up DOS ic concentrated below the Fermi energy. Therefore spin up states are almost filled. For spin down states the DOS is centered at the Fermi energy indicating that they are partially filled. A self consistent density functional calculation shows that there are 7.56 electrons in $3d$ states with a total magnetic moment of 1.70 μ_B per Co which is consistent with a d^8 configuration of Co in the high spin state..

Near the Fermi energy at Γ point the Co d A_1 $(3z^2 - r^2)$ state strongly mixes with Cu sp states. The trigonal crystal field at the surface allows the mixing between Co d and p states since Co is not at the inversion center. This is the difference between the Co/Cu(111) case and the Ag/Ag(111) case where all the $3d$ states are filled for Ag atoms. Although d (especially $3z^2 - r^2$) states cross the Fermi level, they are more compact compare to p states which are also present at E_F. Therefore tunneling could be into p states rather than d states.

The width of the Co d A_1 state is a result of the coupling with the Cu sp surface and bulk states. Also from the spin density plots we notice that Co adatoms polarize nearest Cu layers of the slab by considerable amount. According to LMTO results the second Cu layer has the highest magnetic moment per Cu among all other layers. The spin density distribution is quite anisotropic and it is extended throughout the whole Cu slab. Also at least three Cu layers have significant influence on the electronic properties of Co.

To outline the future direction of this project, we begin by noting that the amount of different orbital characters present in the basis wave function is not known. Therefore this subject needs to be investigated further. Once we can find out important orbital states present in the wave function, a tight binding treatment of the basis set together with at least nearest and next nearest neighbor hopping may help us writing an effective Hamiltonian for the system.

We note that the Co $3d$ spin down states centered at the Fermi energy and especially the Co d $3z^2 - r^2$ states are narrow in energy and the density of states exhibits very sharp structures including a strong dip just below the Fermi energy. This sharply structured density of states would of course also be seen in a STM measurement and so from the present study it is not that clear that a more sophisticated interpretation such as in terms of the Kondo effect are needed. On the other hand we should also realize that the very small width of the d states will cause strong changes in the density of states if we add real correlations to the problem as in the Anderson impurity model including a Hubbard U. If large enough this would again split the d states at the Fermi energy into occupied and unoccupied regions with a gap and then we would be back to a Kondo like problem but very important would then be to take into account the sharp structure in the density of band states needed to produce the sharp structures in the Co d density of states. In other words the problem will be much more complicated than the simple Kondo models usually used. There is another important issue though seen in these calculations and that is the very sharp structure seen in the Co s and p density of states right at the Fermi energy. As has been mentioned in the introduction we expect much larger tunneling matrix elements from a tip to a solid for tunneling involving the Co $4s$ and $4p$ states than for the much more compact 3d states. The density of states of these seen in Fig 4.6 exhibit a sharp dip very close to the Fermi energy with a width of only about 50 meV. This could indicate a different origin of the dip seen in STM than that of the Kondo problem. All these issues should now be studied with appropriate models. LDA+U could be used to see what happens if U is switched on. One should look at the local projected density of states of other adatoms such as Cu or Mn to see if the sharp structure seen very close to E_F is characteristic of Co or is a general effect. In addition an Anderson impurity model should be developed and worked out using the strongly structured density of states and hybridization matrix elements.

Bibliography

[1] H.C. Manoharan, C.P. Lutz, and D.M. Eigler, Nature(London) **403**, 512 (2000).

[2] P.W. Anderson, Phys. Rev. **124**, 1, 41 (1961).

[3] G. Grüner and A. Zawadowski, Rep. Prog. Phys. **37**, 1497 (1974).

[4] A.C. Hewson, *The Kondo problem to Heavy Fermions*, (Cambridge University, Cambridge, England).

[5] J.R. Schrieffer and P.A. Wolff, Phys. Rev. **149**, 2, 491 (1966).

[6] J. Li, W.-D. Schneider, R. Berndt, and B. Delley, 1998, Phys. Rev. Lett. **80**, 2893 (1998).

[7] V. Madhavan, W. Chen, T. Jamneala, M.F. Crommie, and N.S. Wingreen, Science **280**, 567 (1998).

[8] N. Knorr, A. Schneider, and L. Diekhöner, P. Wahl and K. Kern, Phys. Rev. Lett. **88**, 9, 096804-1 (2002).

[9] G.A. Fiete and E.J. Heller, Rev. of Mod. Phys. **75**, 933 (2003).

[10] M.F. Crommie, C.p. Lutz and D.M. Eigler, Science, **262**, 218 (1993).

[11] Fiete, J. S. Hersch, E. J. Heller, H. C. Manoharan, C. P. Lutz, and D. M. Eigler, 2001, Phys. Rev. Lett. **86**, 2392 ().

[12] U. Fano, Phys. Rev. **124**, 1866 (1961).

[13] Újsághy, J. Kohra, L. Szunyogh and A. Zawadowski, Phys. Rev. Lett. **85**, 2557 (2000).

[14] J. Kondo, Prog. Theor. Phys. **32**, 37 (1964).

[15] M. Plihal and J.W. Gadzuk, Phys. Rev. B **63**, 085404-1(2001).

[16] M.A. Schneider, L. Vitali, P. Wahl, N. Knorr, L. Diekhöner, G. Wittich, M. Vogelgesang and K. Kern, Appl. Phys. A **80**, 937 (2005).

[17] L. Limot and R. Brendt, cond-mat/0312434(2003).

[18] P.O. Gartland and B.J. Slagsvold, Phys. Rev. B **12**, 4047 (1975).

[19] J. Tersoff and D.R. Hamann, Phys. Rev. Lett. **50**, 1998 (1985).

[20] J. Tersoff and D.R. Hamann, Phys. Rev. B **31**, 805 (1985).

[21] S.G. Louie, P. Thiry, R. Pinchaux, Y. Petroff, D. Chandesris and J. Lecante, Phys. Rev. Lett. **44**, 549 (1980).

[22] L. Limot, E. Pehlke, J. Kröger and R. Brendt, Phys. Rev. Lett. **94**, 036805-1 (2005).

[23] N.W. Ashcroft and N.D. Mermin, *Solid State Physics*, Harcourt College Publishers, 1976.

[24] F. Mezei and A. Zawadowski, Phys. Rev. B **3**, 1, 167 (1971).

[25] J. Merino and O. Gunnarsson, Phys. Rev. B **69**, 115404 (2004).

[26] L.H. Thomas, Proc. Camb. Phil. Soc. **23**, 542 (1927).

[27] E. Fermi, Atti. Accad. Nazl. Lincei, **6**, 602 (1927).

[28] P. Hohenberg *et al*, Phys. Rev. **136**, B864 (1964).

[29] W. Kohn, Nobel Lecture, Rev. Mod. Phys.**71**, 1253 (1998).

[30] W. Kohn, Proc. Int'l Scoool of Physics, Enrico Fermi, Course LXXXIX, p.4 (1985).

[31] M. Levy, Phys. Rev. A, **26**, 1200 (1982).

[32] E. Lieb, Int. J. Quant. Chem., **24**, 243 (1983).

[33] R.O. Jones and O. Gunnarsson, Rev. Mod. Phys. **61**, 689 (1989).

[34] C.O. Almbladh *et al*, Phys. Rev. B, **31**, 3231 (1985).

[35] O.K. Andersen, Phys. Rev. B, **12**, 3060 (1975).

[36] O. Jepsen, J. Madsen and O.K. Andersen, Phys. Rev. B, **18**, 605 (1978).

[37] P. Blaha, K. Schwarz, G. Madsen, D. Kvasnicka, and J. Luitz, WIEN2k, An Augmented Plane Wave + Local Orbitals Program for Calculating Crystal Properties, (Karl- heinz Schwarz, Techn. Universität Wien, Austria) (1999), ISBN 3-9501031-1-2.

[38] F. Reinert, G. Nicolay, S. Schmidt, D. Ehm, and S. Hüfner, Phys. Rev. B, **63**, 115415 (2001).

[39] W.A. Harrison, *Electronic Structure and the Properties of Solids*, Dover Publications, 1989.

[40] K. Terakura, T. Oguchi, A.R. Williams and J. Kübler, Phys. Rev. B, **30**, 8, 4734 (1984).